DEVELOPMENT AND EVOLUTION OF MAGNETIC FIELDS IN ACTIVE REGIONS ON THE SUN

Thesis by

Dean-Yi Chou

In Partial Fulfillment of the Requirements

for the Degree of

Doctor of Philosophy

California Institute of Technology

Pasadena, California

1987

(Submitted 11 September, 1986)

To my parents

ACKNOWLEDGEMENTS

There are many people to whom I am grateful for assistance and advice through my five years at Caltech. Foremost, I am indebted to Professor Harold Zirin, my advisor, for his constant supervision and encouragement on my work, for many helpful discussions and suggestions, and for wisdom on many matters.

I express my deepest appreciation to Professor Roger D. Blandford for teaching me the ways of learning and conducting research in my first year, and many helpful discussions and suggestions on later work.

It is not possible to list everyone who has guided and helped me. But I am particularly grateful to the other members of my oral examination committee, Professors Peter Goldreich, Marshall Cohen, and Ken G. Libbrecht, for many useful suggestions.

To all the pundits at Caltech who taught me physics and astronomy.

To the research staff in the solar group, Gordon Hurford, Sara Martin, Frances Y. Tang, and Margaret A. Liggett, for helpful discussions and kind support.

To the Big Bear staff, Alan P. Patterson, William Marquette, Randy J. Fear, and other members for kind and useful support on observing and other things.

To David Hough and Bruce D. Popp for reading of drafts, correction of grammar, scientific suggestions, and much more.

To John A. Biretta for providing computer software and solving many problems on the VAX. Without his help, this work would have taken much longer.

To Kwok-Wai Cheung and Pawan Kumar for many delightful and helpful discussions on physics.

To Richard Edelson, my officemate during the last two years, for his noise, nonsense, and, of course, help.

To Haimin Wang, for his cooperation on chapter 2 and other helpful discussions.

To my fellow students for friendship and companionship, in particular in the VAX room, and in the "bat cave" during my first two years.

To the supporting staff in the solar group and the Astronomy Department for their kind support and help.

To Helen Z. Knudsen, the librarian, for her kind assistance, in particular in finding the odd journals.

Finally, I would like to thank everyone at Caltech for providing such an inspiring and exciting atmosphere to work in.

ABSTRACT

The purpose of this thesis is to investigate the development and evolution of magnetic fields in new active regions on the sun. The major observations are digital magnetograms of the line-of-sight component of magnetic fields made with the high sensitivity videomagnetograph at the Big Bear Solar Observatory, and Hα filtergrams with the 1/4 $\AA$ Hα Zeiss filter.

This thesis consists of three themes. First, the separation velocity of emerging magnetic flux is investigated. I measure the separation velocities of opposite polarities of 24 new bipoles, and compare them with the theoretical values estimated by the present theory of magnetic buoyancy. The predicted velocities are higher than those observed. Second, the cooling time scale of growing sunspots is studied. I define the cooling time scale and derive it from the measurements of intensity and magnetic field strength of sunspots. The cooling time scales of the ten growing sunspots studied range from 0.5 to 9 hr. I also estimate the cooling time scale from two models, the Inhibition Model and the Alfven Wave Model, based on linear theory. Both models give cooling times of about 0.05 hr. Third, nonadiabatic effects in convective instabilities in thin flux tubes are examined. I study the convective instabilities in thin flux tubes by including a nonadiabatic term. I find that a flux tube is convectively stable for any field strength.

TABLE OF CONTENTS

CHAPTER 1

INTRODUCTION

Most activity on the sun is dominated by the magnetic field and its interaction with the plasma atmosphere. The magnetic field is commonly thought to be generated by some kind of dynamo mechanism operating in the convective zone. The azimuthal field, generated by differential rotation, is brought to the surface by magnetic buoyancy or supergranular flow. The emerging flux always appears as a bipolar form, with the opposite polarities moving apart during the growth phase. Most new regions stop growing in less than a day, but sometimes magnetic flux continues to emerge and a bipole grows into an active region. Arch filament systems, which connect the opposite polarity fields, are observed in large, growing active regions. Pores or sunspots might be formed over a period of hours or days through the progressive gathering of small flux tubes into a large tube. Many questions concerning the development of active regions still lack a complete explanation, although the above picture is widely accepted. In this thesis, I will investigate three themes: (1) the problem of magnetic buoyancy, which probably carries magnetic fields to the surface of the sun; (2) the cooling mechanism of sunspots; and (3) the nonadiabatic effects in convective collapse, which may be the mechanism for concentrating magnetic field to kilogauss.

Frazier (1972) proposed a model to describe emergence of magnetic fields. In his model, magnetic fields are carried up to the surface of the sun by supergranular flow. This model is based on observations that emerging magnetic fields first appear near the center of a supergranule. However, it is difficult to identify a supergranule cell without velocity field measurements because, first, the magnetic network may not exactly correspond to supergranule cells in active regions; secondly, even in the quiet sun, there is no one-to-one correspondence between the magnetic network and the supergranule (Wang 1986). Two or more supergranule cells may correspond to one cell of the magnetic network. Thus, a dopplergram is

required to identify a supergranule cell. All previous observations of emergence of magnetic flux do not have velocity fields taken simultaneously. In six of our eight emerging regions for which dopplergrams are available, the new flux emerges at the boundaries of supergranules (Chapter 2). Therefore, the supergranular flow can not be a major mechanism to carry magnetic field to the surface.

Another possible mechanism to carry magnetic field to the surface is magnetic buoyancy. Many authors have investigated the theory of magnetic buoyancy. Parker (1955) first proposed the mechanism of magnetic buoyancy. Parker (1975a, 1979b), Unno and Ribes (1976), Schüssler (1977) and Moreno-Insertis (1983) calculate the time for a horizontal flux tube, of which radius is assumed to be much smaller than the pressure scale height, to cross the convective zone by magnetic buoyancy. Schüssler (1979) considers a flux tube with a radius comparable to or greater than the pressure scale height. Tsinganos (1980) investigates instabilities of a buoyant flux tube. Van Ballegooijen (1982) discusses a flux tube rooted in the stable layer below the convective zone. So far there has been no theoretical discussion about the emerging velocity of a flux tube in the photosphere and the chromosphere in which observations are made, and few observations have been made to test the theory.

In the chromosphere, arch filaments, which trace out flux tubes, are observed to be fairly low-lying (Roberts 1970). Their summit has blueshifts up to 10 km/s, while footpoints have redshifts up to 50 km/s (Bruzek 1967, 1969; Roberts 1970). The common interpretation is that the summit of the flux tube rises, while plasma falls down along the flux tube due to gravity. But there is no further investigation of the mechanism which causes the summit to rise with such a high velocity. It can not be simply caused by buoyancy, since the internal density is higher than ambient density. Nor can it be due to the lateral motion of the footpoints, since

the lateral velocity of the footpoints is only about 1 km/s. Further observational and theoretical investigations are needed.

At the photosphere, the most direct information about the emerging mechanism comes from vertical velocity measurement. Kawaguchi and Kitai (1976) report an upper limit of 0.2 km/s for the rising velocity of the flux tube. However, Brants (1985) reports an upward velocity of about 1 km/s near the line of inversion in emerging flux regions. Harvey and Martin (1973) and Born (1974) measure the separation velocity of the opposite polarities of ephemeral regions and emerging flux regions. In chapter 2, I measure the separation velocity and other quantities (such as magnetic flux and size) of 24 new bipoles. The measured separation velocities range from about 0.2 to 1 km/s. The fluxes of the bipoles range over more than two orders of magnitude, and the mean field strength and the sizes range over one order of magnitude. I also estimate the separation velocity at the photosphere from the theory of magnetic buoyancy, which is higher than the observed values. Although the present theoretical values do not agree with the observed ones, this work serves as a start and provides preliminary information on the emerging mechanism.

After magnetic flux emerges, pores or sunspots might be formed over a period of hours or days by gathering small magnetic knots together. The sunspots are cooler than their surroundings, and have high field strength up to 3500 Gauss. The mechanism for causing the low temperature of sunspots is one of the oldest problems in solar physics. Two different mechanisms, the Inhibition Model and the Alfven Wave Model, have been proposed. In the Inhibition Model, first proposed by Biermann (1941), the convection which carries energy to the photosphere is partially inhibited by magnetic fields. In the Alfven Wave Model, thermal energy is transformed into mechanical energy. In the presence of a magnetic field, if

the thermal conductivity is greater than the magnetic diffusivity, a temperature gradient can cause overstable modes of Alfven waves (or more complicated magnetoacoustic waves), which can carry a large amount of energy away (Parker 1979a and references cited therein). So far most theoretical work has been time independent. In Chapter 3, I propose a method to provide dynamical information on the cooling mechanism of sunspots, which is the cooling time scale.

Observations show that the effective temperature of sunspots is a function of their field strength (Bray and Loughhead 1964; Deinzer 1965; Dicke 1970). As a sunspot grows, its field strength increases and intensity decreases. My observations show that during the growth phase, a new sunspot has a higher intensity than a stable sunspot of the same field strength. Therefore, it must take time for a growing sunspot to reach an equilibrium state. From the time history of intensity and field strength of growing sunspots and the relationship between intensity and field strength of stable sunspots, I derive the cooling time of growing sunspots. The cooling time scale is defined as the rate of change of the intensity at a fixed magnetic field strength. Therefore, it is independent of the mechanism which causes increases of magnetic field, and it is also independent of whether or not a sunspot consists of a number of unresolved flux tubes. The cooling time scales of the ten growing sunspots studied range from 0.5 to 9 hours. I also estimate the cooling times from two models, based on linear theory. Both models give a time scale of about 0.05 hour. The discrepancy between theoretical and observed values may be due to the fact that the observed sunspots are in the nonlinear regime while the theoretical estimate is done in the linear regime. A calculation better than the order of magnitude estimate is required in order to make comparisons with observed values.

One of the most exciting discoveries in solar physics in the last two decades is

that most photospheric magnetic fields outside sunspots are concentrated in small elements with field strength of about 1500 Gauss (see a review paper by Harvey 1977 and references cited therein), while the average field is only a few Gauss over the entire surface of the sun and about one hundred Gauss in active regions. Two questions immediately arise: How does a flux tube maintain its equilibrium? What concentrates magnetic fields to kilogauss in the first place?

Parker (1955, 1975b) points out that an equilibrium flux tube is subjected to the hydromagnetic exchange instability. Meyer *et al.* (1977) show that the magnetic buoyancy can stabilize the exchange instability in the upper, rapidly flaring part of the flux tube.

Since the discovery of concentration of magnetic fields, many mechanisms of concentration have been proposed. They can be grouped into two categories: the dynamical mechanism and the thermal mechanisms. The dynamical mechanisms include: (1) concentration by the convection of granules or supergranules (Parker 1963, 1973a,b, 1979b, 1981; Weiss 1964, 1977; Meyer *et al.* 1974; Galloway *et al.* 1977; Pecker and Weiss 1978; Galloway and Moore 1979); (2) concentration by turbulence and the Bernoulli effect (Parker 1974a,b, 1979b, 1981; Zwaan 1978); (3) concentration by twisting (Piddington 1976a,b,c; Parker 1981). Parker (1976, 1979b, 1981) has shown that the above dynamical mechanisms fail to concentrate magnetic fields to kilogauss at the photosphere.

The thermal mechanisms have been shown to be promising means to produce kilogauss flux tubes by many authors(Parker 1976, 1978, 1979b, 1981; Galloway *et al.* 1977; Spruit 1979; Spruit and Zweibel 1979; Unno and Ando 1979; Venkatakrishnan 1983, 1985). The idea of a thermal mechanism is described as follows: The plasma flowing adiabatically downward within a flux tube is cooler than its surroundings because the convective zone is superadiabatic. This temperature

reduction could cause the pressure scale height to be smaller and the density higher inside the flux tube, which would lead the plasma to continue to flow downward; that is, an instability would occur in the flux tube. This instability is essentially the same as the ordinary convective instability caused by a steep temperature gradient. The difference is that the plasma inside a flux tube is guided along the tube by the magnetic field, and it does not exchange heat with its surroundings, nor does it mix with its surroundings; that is, it does not circulate as in ordinary convection. Instead, it continues to flow along the flux tube. The downward motion would evacuate the plasma inside the tube and concentrate the magnetic field. Spruit (1979) and Spruit and Zweibel (1979) use a model of the solar atmosphere to show that a flux tube with photospheric field strength less than about 1300 Gauss is convectively unstable, and would collapse into an equilibrium state of higher field strength. These works demonstrate that magnetic fields could be concentrated into small flux tubes of kilogauss by the thermal mechanism (convective collapse). The above calculations are based on the assumption that the perturbation is adiabatic. Venkatakrishnan (1985) shows that the mechanism of concentration of flux tubes by convective collapse becomes less efficient when radiative heat transport is included.

In Chapter 4, I consider a nonadiabatic effect caused by the change of the magnetic field. This is based on the observational fact that sunspots with stronger magnetic field have lower effective temperature (or less heat content). By including this nonadiabatic effect, I find that flux tubes of any field strength are stable against the convective collapse discussed by Spruit and Zweibel (1979).

The radius of a small flux tube is less than 300 km, which can not be resolved by present observations. The observational results indicating kilogauss rely heavily on the indirect calculation. Furthermore, it is not clear whether *all* magnetic fields at the photosphere are concentrated in small tubes of kilogauss (Simon and Zirker

1974; Wang *et al.* 1985; Zirin 1985). My result shows that flux tubes of any field strength might be stable against convective collapse, although whether or not they actually exist is a matter to be settled by observation.

REFERENCES

Biermann, L. 1941, *Vierteljahrsschr. Astr. Gesellsch.*, **76**, 194.

Born, R. 1974, *Solar Phys.*, **38**, 127.

Brants, J. J. 1985, *Solar Phys.*, **98**, 197.

Bray, R. J. and Loughhead, R. E. 1964, *Sunspots* (New York: Dover) .

Bruzek, A. 1967, *Solar Phys.*, **2**, 451.

Bruzek, A. 1969, *Solar Phys.*, **8**, 29.

Deinzer, W. 1965, *Ap. J.*, **141**, 548.

Dicke, R. H. 1970, *Ap. J.*, **159**, 25.

Frazier, E. N. 1972, *Solar Phys.*, **26**, 130.

Galloway, D. J., Proctor, M. R. E., and Weiss, N. O. 1977, *Nature*, **266**, 686.

Galloway, D. J. and Moore, D. R. 1979, *Geophys. Astrophys. Fluid Dynamics*, **12**, 73.

Harvey, J. W. 1977, *Highlight of Astronomy*, ed. E. A. Müller, **4**, Part II, p. 223.

Harvey, K. L. and Martin, S. F. 1973, *Solar Phys.*, **32**, 389.

Kawaguchi, I. and Kitai, R. 1976, *Solar Phys.*, **46**, 125.

Meyer, F., Schmidt, H. U., Weiss, N. O., and Wilson, P. R. 1974, *M. N. R. A. S.*, **169**, 35.

Meyer, F., Schmidt, H. U., and Weiss, N. O. 1977, *M. N. R. A. S.*, **179**, 741.

Moreno-Insertis, F. 1983, *Astron. Astrophys.*, **122**, 241.

Parker, E. N. 1955, *Ap. J.*, **121**, 491.

Parker, E. N. 1963, *Ap. J.*, **138**, 552.

Parker, E. N. 1973a, *Ap. J.*, **186**, 643.

Parker, E. N. 1973b, *Ap. J.*, **186**, 665.

Parker, E. N. 1974a, *Ap. J.*, **189**, 563.

Parker, E. N. 1974b, *Ap. J.*, **190**, 429.

Parker, E. N. 1975a, *Ap. J.*, **198**, 205.

Parker, E. N. 1975b, *Solar Phys.*, **40**, 291.

Parker, E. N. 1976, *Ap. J.*, **204**, 259.

Parker, E. N. 1978, *Ap. J.*, **221**, 368.

Parker, E. N. 1979a, *Ap. J.*, **230**, 905.

Parker, E. N. 1979b, *Cosmical Magnetic Fields* (New York: Oxford), Chap. 8 and 10.

Parker, E. N. 1981, *Solar Phenomena in Stars and Stellar Systems*, ed. R. M. Bonnet and A. K. Dupree (Dordrecht: Reidel), p. 33.

Peckover, R. S. and Weiss, N. O. 1978, *M. N. R. A. S.*, **182**, 189.

Piddington, J. H. 1976a, *Astrophys. Space Sci.*, **40**, 73.

Piddington, J. H. 1976b, *Astrophys. Space Sci.*, **45**, 47.

Piddington, J. H. 1976c, *IAU Symposium No. 71, Basic Mechanisms of Solar Activity*, ed. V. Bumba and J. Kleczek (New York: John Wiley), p. 389.

Roberts, P. H. 1970, *'Velocity Fields in Magnetically Disturbed Regions of the Hα Chromosphere'*, Thesis, Calif. Inst. of Technology.

Spruit, H. C. 1979, *Solar Phys.*, **61**, 363.

Spruit, H. C. and Zweibel, E. G. 1979, *Solar Phys.*, **62**, 15.

Schüssler, M. 1977, *Astron. Astrophys.*, **56**, 439.

Schüssler, M. 1979, *Astron. Astrophys.*, **71**, 79.

Simon, G. W. and Zirker, J. B. 1974, *Solar Phys.*, **35**, 331.

Tsinganos, K. C. 1980, *Ap. J.*, **239**, 746.

Unno, W. and Ando, H. 1979, *Geophys. Astrophys. Fluid Dynamics*, **12**, 107.

Unno, W. and Ribes, E. 1976, *Ap. J.*, **208**, 222.

van Ballegooijen, A. A. 1982, *Astron. Astrophys.*, **106**, 43.

Venkatakrishnan, P. 1983, *J. Astrophys. Astr.*, **4**, 135.

Venkatakrishnan, P. 1985, *J. Astrophys. Astr.*, **6**, 21.

Wang, J., Zirin, H. and Shi, Z. 1985, *Solar Phys.*, **98**, 241.

Wang, H. 1986, in preparation.

Weiss, N. O. 1964, *M.N.R.A.S.*, **128**, 225.

Weiss, N. O. 1977, *Highlight of Astronomy*, ed. E. A. Müller, 4, Part II, p. 241.

Zirin, H. 1985, *Aust. J. Phys.*, **38**, 961.

Zwaan, C. 1978, *Solar Phys.*, **60**, 213.

CHAPTER 2

THE SEPARATION VELOCITY OF EMERGING MAGNETIC FLUX

Submitted to Solar Physics

ABSTRACT

We measure the separation velocity of opposite poles from 24 new bipoles on the sun. We find that the measured velocities range from about 0.2 to 1 km/s. The magnetic fluxes of the bipoles range over more than two orders of magnitude, and the mean field strength and the sizes range over one order of magnitude. The measured separation velocity is not correlated with the flux nor with the mean field strength. A calculation based on the current theory of magnetic buoyancy shows that the separation velocity is between $7.4\,B\,a^{-1/4}\,cot\theta$ and $13\,cot\theta$ km/s (θ is the elevation angle of the flux tube at the photosphere, a is the radius), which does not agree with measurements, unless the flux tubes are almost vertical. The predicted rising velocity, which is between $3.7\,B\,a^{-1/4}$ and 6.5 km/s, is also higher than the measured vertical velocity near the line of inversion in emerging flux regions. It is likely that the current theory is too simplified for application to the sun.

I. INTRODUCTION

Observations have shown that some magnetic fields on the sun emerge from below the photosphere. The mechanism responsible for bringing magnetic fields to the solar surface has long been believed to be magnetic buoyancy, which was first introduced by Parker (1955). Since then, many theoreticians (Parker 1975, 1979; Unno and Ribes 1976; Schüssler 1977, 1979; Tsinganos 1980; van Ballegooijen 1982; Moreno-Insertis 1983) have contributed to this hypothesis. But few observations have been made to provide information for testing the theory. Kawaguchi and Kitai (1976) report: " We have not observed the single blue shift of Fraunhofer lines in the region corresponding to dark lanes in between the developing sunspot pores; we expect that the velocity of rising loops is not larger than the mean errors (0.2 km/s) of our measurements of radial velocities." However, Brants (1985) reports that an upward velocity of about 1 km/s is found near the line of inversion in emerging flux regions. Other authors (Harvey and Martin 1973; Born 1974) measure the separation velocities of opposite poles of ephemeral regions and emerging flux regions.

In this paper, we measure the separation velocities and magnetic fluxes of 24 emerging bipoles, and compare them with the values estimated from the present theory of magnetic buoyancy to provide preliminary information on the emerging mechanism. In section II, we discuss the measurements of the separation velocities and other quantities of 24 emerging bipoles. In section III and IV, we discuss the present theory of magnetic buoyancy and the buoyant velocity. In section V, we compare the theoretical values with the observed ones and discuss other possible theories.

II. OBSERVATIONS AND RESULTS

Emerging magnetic fields on the sun always appear as new bipoles, with the opposite polarities moving apart during the growth phase. The new regions have a broad spectrum of size, flux and lifetime. Some of these new regions are designated as emerging flux regions (EFR), which are defined as the first stage of active regions (Zirin 1972). They might develop into large active regions with flux of about 10^{22} Maxwell, and last for several solar rotations. Some of these new regions are ephemeral regions (Harvey and Martin 1973; Martin *et al.* 1984) with flux of only 10^{18} Maxwell, and last for only a few hours. Even though ephemeral regions may have some properties (for example, flux, size, numbers and distribution) different from emerging flux regions, in this paper we consider them as the same entity. We classify them only by the amount of flux they develop.

We have observed 24 new bipoles with the high sensitivity videomagnetograph and the 1/4 $\AA$ Hα Zeiss filter at the Big Bear Solar Observatory. The videomagnetograph has been described by Martin (1983), Zirin (1985) and Shi (1986). The digital magnetograms are taken at rates of about 10 to 30 per hour, depending on integration time. The high spatial resolution Hα pictures are taken at a rate of about about 4 per minute. The observed quantities of these new bipoles are listed in Table 1, and explained as follows:

(1) Separations

We define two different separations of the opposite poles of a new bipole. The first one, the separation of maxima, is the distance between the maxima of the opposite polarity fields. The second one, the separation of borders, is the distance between the outer borders of two poles. The separation of maxima can be measured more accurately than the separation of borders, but the latter has better physical meaning, because the position of the maxima might be affected by the development

of a new stronger pole. The velocities derived from the two different separations will be discussed in (2). The geometric projection has been corrected such that all regions are transformed to the center of the solar disk for comparison on the same base. Plots of the separations of maxima *versus* time of two typical new bipoles are shown in Figures 1a and 2a. For some regions (e.g. Figure 2a), the position of the emerging flux is difficult to define at a very early stage and the measured separation has a larger error. Otherwise, the error is about 1 to 2 arcsec.

(2) Separation Velocities

The separation increases nearly linearly with time over a certain period. Usually, the slope of the curve decreases with time. We define the separation velocity as the slope of a linear fit of the *steepest* portion of the curve (as shown in Figures 1a and 2a). The choice of the steepest portion is made by eye. The variation in the beginning of Figure 2a is caused by the uncertainty in defining the position of the emerging flux upon first appearance. This portion of the curve is not included in the determination of the separation velocity. Because of the high temporal resolution, the velocity can be determined accurately. The error caused by the choice of the steepest portion of the curve is usually less than 30%. Both the separation velocity of maxima (v_m) and the separation velocity of borders (v_b) are measured and shown in Table 1. A plot of v_b *versus* v_m is shown in Figure 3. They are nearly the same. Hereinafter, we use the "separation velocity" to refer to the separation velocity of maxima. The separation velocity *versus* the magnetic flux (defined in (4)) and the mean field strength (defined in (8)) are plotted in Figures 4 and 5 respectively. Figures 4 and 5 show that the separation velocity is not correlated with the flux and the mean field strength of the region. From the theory of magnetic buoyancy, the emerging velocity, which is related to the separation velocity, is a function of magnetic field strength and cross section of the

flux tube. The measured velocities range from about 0.2 to 1 km/s. The fluxes of the bipoles range over more than two orders of the magnitude, and the mean field strength and the sizes range over one order of the magnitude. We will discuss the theory of magnetic buoyancy in Section III and IV.

Some of the bipoles are observed from birth, but we do not find the separation velocity to be as high as 2 km/s reported by Born (1974), and 5 km/s by Harvey and Martin (1973). We argue that first, as the bipole first emerges, the position of the emerging flux can not be accurately defined; secondly, high temporal resolution is required to accurately measure the separation velocity in the first few minutes because of the error in the position measurement. Frazier (1972) reports transverse velocities of 0.1 to 0.4 km/s of 26 magnetic knots in an active region. These correspond to separation velocities of 0.2 to 0.8 km/s, which are consistent with our results.

(3) Initial Separations and Mean Separations

The initial separation is the separation of maxima we first observe for the bipole. For the regions that we observe from the very beginning of emergence, we define the initial separation as when we first can identify the bipolar feature. For those in which we miss the very beginning of emergence, we simply define the initial separation as the first observed one. The initial separation indicates how early we start observing the new bipole. The mean separation is the separation of maxima averaged over the period in which the separation velocity is defined. Both are shown in Table 1. There is no apparent correlation between separation velocity, v_m, and mean separation and initial separation.

(4) Magnetic Flux

For some new bipoles, the fluxes of two poles are not equal. The same phenomenon is also reported by other authors (Topka and Tarbell 1983; Wilson and

Simon 1983; Simon and Wilson 1985). The possible explanations are geometry of the fields, instrumental limitations and effects, seeing effects, the surface dynamo (Akasofu 1984; Simon and Wilson 1985), and the cancellation of the flux coincident with its first appearance (Livi *et al* 1985). Plots of the fluxes of both poles *versus* time for the two regions are shown in Figures 1b and 2b. We define mean flux in Table 1 as an average over the period in which the separation velocity is defined for each polarity, and then take the average of two opposite polarities.

(5) Arch Filaments

Some regions show arch filament systems in $H\alpha$ filtergrams. Table 1 shows that there is a threshold flux for an arch filament system, which is about $0.5 \times 10^{20} - 1.0 \times 10^{20}$ Maxwell. Harvey and Martin (1973) suggest that a threshold of about 0.75×10^{20} Maxwell is needed to support an arch filament system.

(6) Pores

Some regions have visible pores or sunspots in white-light pictures or off-band Hα filtergrams during the observing period. Table 1 shows that a minimum flux of about 10^{20} Maxwell is found for a pore. Since the visibility of pores very much depends on the seeing, there is the possibility that we miss them in some cases. A minimum flux of 0.25×10^{20} Maxwell for a pore has been reported by other authors (Zwaan 1978).

(7) Radii

We define the radius as the average of major and minor axes of the 40 Gauss field strength contour of each polarity, then we take the average of two opposite polarities. The geometric projection has also been corrected such that all regions are transformed to the center of the solar disk. There is no apparent correlation between separation velocity, v_m, and radius.

(8) Mean Field Strength

The line-of-sight component of mean field strength, $B_{//}^{(mean)}$, is defined as observed flux divided by observed area.

III. BUOYANT FORCES

In this section, we review some points of magnetic buoyancy relevant to our discussion. In Section IV, we calculate the buoyant velocity at the photosphere.

Magnetic buoyancy brings azimuthal fields to the surface of the sun. For the deep part of the convective zone, the radius of flux tubes is much less than the pressure scale height, and therefore, the variations of pressure, density and temperature across the radius can be ignored. But as a flux tube approaches the surface, it expands rapidly while the scale height decreases at the same time (Schüssler 1979). In the upper part of the convective zone, the radius of the tube can be greater than the scale height. For example, at the photosphere, the scale height is only about 200 km, while the cross section of an emerging bipole can be few thousand km. Therefore, we can not ignore the variations of pressure, density and temperature across the tube. In the following discussion, we consider two limits: the radius (a) much less than the scale height (Λ) and $a \gg \Lambda$.

$a)\ a \ll \Lambda$

For a horizontal flux tube, the buoyant force per unit length is proportional to the difference between external density and internal density:

$$F_b = \pi a^2 g (\rho_e - \rho_i), \tag{1}$$

where subscripts e and i refer to external and internal, respectively. For a flux tube of radius a, pressure equilibrium between the flux tube and its surroundings is established on a time scale, $a/\sqrt{V_A^2 + c_s^2}$, where V_A and c_s are Alfven speed and sound speed, respectively. For $a \ll \Lambda$, $a/\sqrt{V_A^2 + c_s^2} \ll \Lambda/v$, where v is

the upward velocity of the flux tube, which is less than c_s and V_A. Therefore, we can assume that at all times the flux tube is in pressure equilibrium with its surroundings:

$$p_e = p_i + \frac{B^2}{8\pi}. \tag{2}$$

By using the ideal gas law, equation (1) can be written as:

$$F_b = \pi a^2 g \rho_e \{1 - \frac{T_e}{T_e + \Delta T} \cdot (1 - \frac{B^2/8\pi}{p_e})\}, \tag{3}$$

where $\Delta T = T_i - T_e$.

If the flux tube is in thermal equilibrium with its surroundings, that is, $\Delta T = 0$, then the buoyant force is

$$F_b = \pi \frac{a^2}{\Lambda} \frac{B^2}{8\pi}. \tag{4}$$

If the flux tube moves adiabatically, the temperature difference, ΔT, is (Parker 1979)

$$\begin{aligned} \Delta T(z) &= \int_{z_o}^{z} \{(\frac{dT_i}{dz'}) - (\frac{dT_e}{dz'})\}\, dz' + \Delta T(z_o) \\ &= \frac{m_H\, g}{k_B} \int_{z_o}^{z} \{\mu_e(z')\, \nabla(z') - \mu_i(z')\, \nabla_{ad}(z')\}\, dz' + \Delta T(z_o), \end{aligned} \tag{5}$$

where $\nabla = \partial \ln T_e / \partial \ln p_e$, $\nabla|_{ad} = \partial \ln T / \partial \ln p|_{ad}$, and μ_e and μ_i are external and internal mean molecular weights, respectively. Since the effect of pressure and temperature on mean molecular weight is small, we assume $\mu = \mu_e = \mu_i$. If we further assume that the initial temperature difference, $\Delta T(z_o)$, is zero,

$$\Delta T(z) = \frac{m_H\, g\, \mu}{k_B} \int_{z_o}^{z} \delta(z')\, dz', \tag{6}$$

where $\delta = \nabla - \nabla_{ad}$. The temperature difference, $\Delta T(z)$, can be computed from a model of the convective zone (e.g. Spruit 1974). Since δ is negligibly small in the deep convective zone, ΔT is not sensitive to the choice of the initial position,

z_o. Using the convection zone model of Spruit and choosing $z_0 = -5000km$, we calculate $\Delta T(z)$; it is plotted in Figure 6.

In equation (3), both the temperature difference and magnetic field contribute to the buoyant force. The buoyant force caused by the temperature difference is just the ordinary convective buoyancy; the buoyant force caused by the magnetic field is the magnetic buoyancy. From Figure 6, $\Delta T \simeq 3000K$ at the photosphere, and $T_e/(T_e + \Delta T) \simeq 0.6$ in equation (3); at a depth of 300 km, $\Delta T \simeq 900K$, and $T_e/(T_e + \Delta T) \simeq 0.93$ in equation (3). Thus, the buoyant force caused by the temperature difference is negligible compared with that caused by the magnetic field, except at the photosphere. But, at the photosphere, the tube is no longer thermally isolated, because energy transport by radiation becomes efficient. Therefore, the buoyant force caused by the temperature difference can be ignored. In the following calculation, we set $\Delta T = 0$ for all z.

$$b)\ a \gg \Lambda$$

Schüssler (1979) shows that, if (i) there is hydrostatic equilibrium inside and outside the tube, respectively, (ii) the magnetic field is uniform inside the tube, (iii) $T_i(z) = T_e(z) =$ constant, and (iv) there is pressure balance at the bottom of the horizontal tube, then the buoyant force per unit length is

$$F_b = \frac{1}{4} B^2 a\, e^{\frac{-a}{\Lambda}} I_1(\frac{a}{\Lambda}), \tag{7}$$

where I_1 is the modified Bessel function of order 1. In the limit $a \ll \Lambda$, equation (7) reduces to equation (4). In the limit $\Lambda \ll a$,

$$F_b \simeq \frac{B^2}{4\sqrt{2\pi}} \sqrt{a\,\Lambda} \tag{8}$$

Schüssler (1979) shows that equation (4) can be used if $a < 0.5\Lambda$, equation (8) if $a > 5\Lambda$.

If the flux tube moves adiabatically, $T_i \neq T_e$. Equation (7) is modified to

$$F_b = \frac{1}{4} B^2 a e^{\frac{-a}{\Lambda_i}} I_1(\frac{a}{\Lambda_i}) + 2\pi a p_{eo} \{e^{\frac{-a}{\Lambda_e}} I_1(\frac{a}{\Lambda_e}) - e^{\frac{-a}{\Lambda_i}} I_1(\frac{a}{\Lambda_i})\}, \quad (9)$$

where $\Lambda_i = kT_i/\mu m_H g$, $\Lambda_e = kT_e/\mu m_H g$, and p_{eo} is the external pressure at the bottom of the horizontal tube. In the limit $a \ll \Lambda_i$ *and* Λ_e, equation (9) reduces to equation (3). In the limit $a \gg \Lambda_i$ *and* Λ_e,

$$F_b \simeq \frac{B^2}{4\sqrt{2\pi}} \sqrt{a\Lambda_i} + \sqrt{2\pi} p_{eo} \sqrt{a\Lambda_i} (\sqrt{\frac{T_e}{T_i}} - 1). \quad (10)$$

IV. BUOYANT VELOCITY

The velocity of a horizontal tube is determined by the buoyant and drag forces. The drag force per unit length of a cylinder can be written as

$$F_d = \frac{1}{2} \rho_e v^2 C_d \cdot 2\, a, \quad (11)$$

where C_d is the drag coefficient, which is well known from experiments for Reynolds numbers, $R_e = 2av/\nu$, between 10^{-1} and 10^6 (Tritton 1977). If the Reynolds number is much less than 1, the drag force can be expressed analytically as (Landau and Lifshitz 1959)

$$F_d = \frac{4\pi \rho_e \nu v}{0.5 - \gamma - \ln(a v/4\nu)}, \quad (12)$$

where $\gamma \simeq 0.577$. Therefore, first we have to determine the value of the Reynolds number.

In the turbulent convection zone, the effective turbulent kinematic viscosity, ν_t, can be approximated by $v_t l/3$, where v_t is the characteristic velocity of turbulence, and l is the characteristic length scale of turbulence (Parker 1979). Since the molecular kinematic viscosity is much smaller than the effective turbulent kinematic viscosity in the solar convective zone and atmosphere, we can ignore

the molecular kinematic viscosity. The characteristic length scale, l, is different for different sizes of the tube. We define a_c and v_c as the size and velocity of the largest eddies, which are granules. From observations, $a_c \simeq 1000km > \Lambda$, $v_c \simeq 1km/s$.

$$a)\ a < \Lambda < a_c$$

Since eddies of size comparable to the cross section of the tube are the most effective in braking the motion, we set l equal to a (Moreno-Insertis 1983). From Kolmogorov's law, we can relate the characteristic velocity to the velocity of the largest eddies,

$$v_t = v_c (\frac{a}{a_c})^{\frac{1}{3}}. \tag{13}$$

The Reynolds number is

$$R_e \simeq 6 \cdot \frac{v}{v_c} \cdot (\frac{a_c}{a})^{\frac{1}{3}}. \tag{14}$$

From observations, $v \simeq 1km/s$, $v_c \simeq 1km/s$, and $a_c \simeq 1000km \simeq 5\Lambda$ at the photosphere. For $a < \Lambda$, $Re > 10$. The drag force is expressed by equation (11). From experiments (Tritton 1977), C_d is about 1. From equations (4) and (11),

$$v = V_A \cdot (\frac{\pi}{2\,C_d})^{\frac{1}{2}} \cdot (\frac{a}{\Lambda})^{\frac{1}{2}}, \tag{15}$$

where $V_A = B/\sqrt{4\pi\rho_e}$.

$$b)\ a > a_c > \Lambda$$

If a is greater than the size of the largest eddies, a_c, and scale height, Λ, then $l \simeq a_c$ and $v_t \simeq v_c$. The Reynolds number is

$$R_e \simeq 6 \frac{v}{v_c} \frac{a}{a_c}. \tag{16}$$

For $a > a_c$ and $v \simeq v_c$, $R_e > 6$. The drag force is expressed by equation (11),

and C_d is of order 1. From equations (8) and (11),

$$v = V_A \cdot (\frac{\pi}{2\,C_d^2})^{\frac{1}{4}} \cdot (\frac{\Lambda}{a})^{\frac{1}{4}}. \tag{17}$$

In the above discussions, we consider the tube to be horizontal. If the tube is curved, the buoyant force is balanced by the magnetic tension and the drag force. But the magnetic tension (F_t) is negligible compared with the the buoyant force, which can be shown as follows. The magnetic tension is

$$F_t = \pi\, a^2 \cdot \frac{B^2}{4\pi\, R}, \tag{18}$$

where R is the radius of the curvature of the tube. From equations (4), (8), and (18), the ratios of the magnetic tension to the buoyant force are Λ/R and $(2\pi)^{1/2}(a/\Lambda)^{1/2}(a/R)$ for $a \ll \Lambda$ and $a \gg \Lambda$, respectively. In general, Λ and a are much less than R. Therefore, we can ignore the magnetic tension, and consider that the tube is straight locally. The effect of magnetic tension will be discussed in section V. If a tube has an elevation angle, θ, at the photosphere instead of being horizontal (see Figure 9), the apparent separation velocity of two poles at the photosphere is different from equations (15) and (17) by a factor $2 \cdot cot\theta$ (shown in the Appendix). The apparent separation velocity of two poles is

$$v = 2\,cot\theta \cdot V_A \cdot (\frac{\pi}{2\,C_d})^{\frac{1}{2}} \cdot (\frac{a}{\Lambda})^{\frac{1}{2}}, \tag{19}$$

if $a < \Lambda$; and

$$v = 2\,cot\theta \cdot V_A \cdot (\frac{\pi}{2\,C_d^2})^{\frac{1}{4}} \cdot (\frac{\Lambda}{a})^{\frac{1}{4}}, \tag{20}$$

if $a > \Lambda$.

V. DISCUSSION

From Table 1, the measured separation velocities range from about 0.2 to 1 km/s. The fluxes of the bipoles range over more than two orders of magnitude, and the mean field strength and the sizes range over one order of magnitude.

It is widely held that all magnetic fields in active regions are concentrated in small kilogauss flux tubes. We assume that each observed bipole consists of a bundle of small flux tubes of radius about 100 km, and field strength about 1500 Gauss at the photosphere. If the filling factor is much less than 1, each flux tube moves independently. Since the radius of these small tubes is less than the scale height, each flux tube has a separation velocity about $v \simeq 13 \, cot\theta$ km/s at the photosphere from equation (19), assuming that $\Lambda = 200$ km and $C_d = 1$.

If the filling factor is close to 1, the material in between the tubes also moves with the tubes, with the observed bipole behaving like a single tube. The effective field strength is the mean field strength of the bipole, and the radius of the tube is the radius of the observed bipole, which is usually much greater than a_c and Λ. The separation velocity of the two poles is expressed by equation (20). If we choose that $C_d = 1$, $\Lambda = 200$ km, and $\rho_e = 3.2 \times 10^{-7}$, then from equation (20) the separation velocity is

$$v = 7.4 \, B \, a^{-\frac{1}{4}} \, cot\theta \;\; km/s, \tag{21}$$

where B is in units of kilogauss, a is in units of 1000 km, and θ is the elevation angle of the tube at the photosphere. The observed $B_{//}^{(mean)}$ in Table 1 is only the line-of-sight component, which is smaller than the real mean field strength. The observed a in Table 1 is greater than the real radius of the tube because of the geometric projection factor (The geometric projection has been corrected for a such that all regions are transformed to the center of the solar disk). Altogether, if we use the observed values of $B_{//}^{(mean)}$ and a in equation (21), this would give a lower limit for v. The value of $7.4 \, B_{//}^{(mean)} \, a^{-1/4}$, defined as v_o, is shown in the fifth column of Table 1. A plot of v_m *versus* v_o is shown in Figure 7. There is no apparent correlation between v_m and v_o.

The angle calculated by equation (21) with observed values of v_m and v_o gives a lower limit for the elevation angle, θ,

$$\theta \geq tan^{-1}(\frac{v_o}{v_m}). \tag{22}$$

The value of $tan^{-1}(v_o/v_m)$, defined as θ_{min}, is shown in Table 1. There is no apparent correlation between θ_{min} and mean separation as shown in Figure 8.

From the measured mean field strength in Table 1, for most of the regions, the filling factor is about 0.1 to 0.6, which is between the two extremes discussed above. The separation velocity would be between $7.4\,B\,a^{-1/4}\,cot\theta$ and $13\,cot\theta$ km/s; and the elevation angle of the tube at the photosphere would be larger than θ_{min}.

Compared with the observed values of velocity in Table 1 (columns 3 and 4), the theoretical values (column 5) seem too large; or else the tubes must be almost vertical at the photosphere for most of the regions. This seems unlikely because observations show that arch filaments, which trace out flux tubes, are flat in the chromosphere and the corona (Roberts 1970). Nevertheless, it is possible that flux tubes are almost vertical at the photosphere, and turn horizontal in the chromosphere. Furthermore, Kawaguchi and Kitai (1976) report that the velocity of rising loops is less than 0.2 km/s; and Brants (1985) reports that the upward velocity near the line of inversion in emerging flux regions, where flux tubes are horizontal, is about 1 km/s. These are lower than the theoretical values, which lie between $3.7\,B\,a^{-1/4}$ and 6.5 km/s. Altogether, the observed values are lower than the values predicted by the present theory of magnetic buoyancy.

The possible resolutions for the discrepancy between the theoretical and the observed values are as follows: (i) The magnetic tension might be important and partially balances the buoyant force. The magnetic tension can be ignored for $a \ll \Lambda$ because the ratio of magnetic tension to buoyant force, Λ/R, usually is

much less than 1. However, the magnetic tension might be comparable to the buoyant force for $a \gg \Lambda$, if the radius of curvature, R, is not much greater than $(2\pi)^{1/2}(a/\Lambda)^{1/2}a$. Thus, for the case that the filling factor is much less than 1, the predicted velocity, $13\,cot\theta$ km/s, is not changed. But, for the case that the filling factor is close to 1, the predicted velocity, $7.4\,B\,a^{-1/4}\,cot\theta$, could be overestimated, that is, the theoretical lower limit of separation velocity could be smaller than $7.4\,B\,a^{-1/4}\,cot\theta$. This might explain the discrepancy between the predicted and the observed velocities for the case that the filling factor is close to 1, because the predicted velocity is close to the theoretical lower limit, which could be less than $7.4\,B\,a^{-1/4}\,cot\theta$. However, this fails to explain the discrepancy for the case that the filling factor is much less than 1, because the predicted velocity is close to the theoretical upper limit, which is $13\,cot\theta$ km/s and which is much greater than the observed values. (ii) The drag coefficient, C_d, might be greater than 1, which is adopted above. The Reynolds number estimated in Section IV, which is based on the mixing length theory, might be too large. This would cause an underestimate of the value of C_d. For example, if the Reynolds number is 10, $C_d \simeq 3$, and the theoretical value of the velocity decreases by a factor of about 1.7; if the Reynolds number is 1, $C_d \simeq 10$, and the theoretical value of the velocity decreases by a factor of about 3. (iii) The drag force in equation (11), based on the laboratory data, might not be applicable in the case that the radius of the flux tube is comparable to the pressure scale height. (iv) The above calculation is based on the assumption of a circular cross section, whereas in fact the cross section may be deformed (Parker 1979; Schüssler 1979; Tsinganos 1980). The deformation may cause an increase of drag force, that is, the rising velocity may be reduced. (v) The magnetic buoyant force discussed in Section III (equations (3) and (10)) might not be applicable to flux tubes near the surface of the sun. For

example, the assumptions made in deriving equation (10) might not be valid for flux tubes near the surface of the sun. A better theoretical calculation is required.

Van Ballegooijen (1982) estimates the horizontal drift velocity of an adiabatic flux tube by assuming that the flux tube is rooted in the stable layer below the convective zone. Our measurements do not agree with his results on two points: (i) his results show that the horizontal drift velocity is highly dependent on the flux and the field strength of the flux tube; (ii) his estimated values are smaller than our measured ones by more than one order of magnitude.

The other possible mechanism to carry magnetic flux to the solar surface is the motion of supergranulation (Frazier 1972). The horizontal velocity of supergranulation is about 0.3 to 0.5 km/s (Simon and Leighton 1964; Wang 1986). If emerging bipoles are moved by supergranular flow and originate at the center of upwelling of flow, the separation velocity would be twice the horizontal velocity of supergranulation, which is 0.6 to 1.0 km/s. This agrees with the observed values. But this mechanism fails to explain the following. (i) For some regions, the opposite poles move apart more than the size of a supergranule, while supergranules can carry magnetic fields only a distance less than their sizes. (ii) In six of eight bipoles, which are simultaneously observed with the Dopplergraph, the new flux first appears at the boundary of supergranules. Since the flow is downward at the boundary of supergranules, it seems unlikely that magnetic field is moved by supergranular flow.

It is important to mention that preceding spots usually move much faster than following spots (Kiepenheuer 1953). Following spots usually are motionless relative to surroundings, or they move very slowly (Zirin 1986). This implies that something else also controls the rise of flux tubes. A complete model for the emerging mechanism has to be able to explain the asymmetry of motion of

preceding and following spots.

This work only provides very preliminary information on the emerging mechanism. The sample of 24 regions may not be enough to allow any statistical conclusion. More direct observations of the vertical velocity field in between opposite polarities, and better theoretical calculations, such as more accurate buoyant force and drag force for an expanding flux tube of radius comparable to or greater than the pressure scale height near the surface for different filling factors, are needed to test the model of magnetic buoyancy.

VI. SUMMARY

(1) The measured separation velocities of 24 bipoles range from about 0.2 to 1 km/s. The fluxes of the bipoles range over more than two orders of magnitude, and the mean field strength and the sizes range over one order of magnitude. The measured separation velocity is not correlated with the flux and the mean field strength of the bipole, nor is it with any other observed quantity in Table 1.

(2) The separation velocity predicted by the present theory of magnetic buoyancy is between $7.4\,B\,a^{-1/4}\,cot\theta$ and $13\,cot\theta$ km/s, where θ is the elevation angle of the flux tube at the photosphere. The rising velocity of the top of flux tubes predicted by the theory of magnetic buoyancy is between $3.7\,B\,a^{-1/4}$ and 6.5 km/s.

(3) The predicted separation velocities are about one order of magnitude greater than the observed velocities, or else the flux tubes are almost vertical for most regions. There is no correlation between the measured separation velocity, v_m, and the theoretical value, v_o ($7.4\,B\,a^{-1/4}$), as shown in Figure 7.

(4) The predicted rising velocities are also significantly greater than the observed upward velocities.

(5) A complete model of the emerging mechanism has to be able to explain the

asymmetry of motion of preceding and following spots.

This work is done is cooperation with Haimin Wang.

APPENDIX

Consider a flux tube with an elevation angle, θ, at the photosphere (Figure 9). Only the component of F_b perpendicular to the tube, which is $F_b cos\theta$, can move the tube; the component parallel to the tube moves material along the tube. Since all regions have been transformed to the center of the disk, as the tube moves upward (from $\overline{DE}$ to $\overline{GH}$), the apparent displacement of the tube at the photosphere is AB, which is equal to $CB/sin\theta$. Therefore, for each leg of the tube, the apparent horizontal velocity is different from equations (15) and (17) by a factor $cot\theta$. The apparent separation velocity of two legs is twice the horizontal velocity of each leg, so

$$v = 2\,cot\theta \cdot V_A \cdot (\frac{\pi}{2\,C_d})^{\frac{1}{2}} \cdot (\frac{a}{\Lambda})^{\frac{1}{2}}, \qquad (A1)$$

if $a < \Lambda$; and

$$v = 2\,cot\theta \cdot V_A \cdot (\frac{\pi}{2\,C_d^2})^{\frac{1}{4}} \cdot (\frac{\Lambda}{a})^{\frac{1}{4}}, \qquad (A2)$$

if $a > \Lambda$.

REFERENCES

Akasofu, S.-I. 1984, *Planet. Space Sci.*, **32**, 1257.

Born, R. 1974, *Solar Phys.*, **38**, 127.

Brants, J. J. 1985, *Solar Phys.*, **98**, 197.

Frazier, E. N. 1972, *Solar Phys.*, **26**, 130.

Harvey, K. L. and Martin, S. F. 1973, *Solar Phys.*, **32**, 389.

Kawaguchi, I. and Kitai, R. 1976, *Solar Phys.*, **46**, 125.

Kiepenheuer, K. O. 1953, *'The Sun'*, ed. G. P. Kuiper, (Chicago: The University of Chicago Press), p. 322.

Landau, L. D. and Lifshitz, E. M. 1959, *Fluid Mechanics* (London: Pergamon), Chap. 2.

Livi, S. H. B., Wang, J., and Martin, S. F. 1985, *Aust. J. Phys.*, **38**, 222.

Martin, S. F. 1983, *'Sacramento Peak Workshop on Small Scale Dynamical Processes'*, (Sunspot, NM: Sacramento Peak Observatory), p. 30.

Martin, S. F., Livi, S. H. B., Wang, J., and Shi, Z. 1985, *'Measurements of Solar Vector Magnetic Fields'*, NASA Conference Publication 2374, ed. M. J. Hagyard, (Washington DC: NASA), p. 403.

Moreno-Insertis, F. 1983, *Astron. Astrophys.*, **122**, 241.

Parker, E. N. 1955, *Ap. J.*, **121**, 491.

Parker, E. N. 1975, *Ap. J.*, **198**, 205.

Parker, E. N. 1979, *Cosmical Magnetic Fields* (New York: Oxford), Chap. 8 and 10.

Roberts, P. H. 1970, *'Velocity Fields in Magnetically Disturbed Regions of the Hα Chromosphere'*, Thesis, Calif. Inst. of Technology.

Schüssler, M. 1977, *Astron. Astrophys.*, **56**, 439.

Schüssler, M. 1979, *Astron. Astrophys.*, **71**, 79.

Shi, Z., Wang, J. and Patterson, A. 1979, *'Calibration of Dopplergrams and Magnetograms at BBSO'*, BBSO Preprint, No. 257, Calif. Inst. of Technology.

Simon, G. W. and Leighton, R. B. 1964, *Ap. J.*, **140**, 1120.

Simon, G. W. and Wilson, P. R. 1985, *Ap. J.*, **295**, 241.

Spruit, H. C. 1974, *Solar Phys.*, **34**, 277.

Topka, K. and Tarbell, T. 1983, in *Small-Scale Dynamical Processes in Quiet Stellar Atmospheres*, Proc. Nat. Solar Obs. Conf., ed. S. Keil (Sunspot, NW:NSO), pp. 278-286.

Tritton, D. J. 1977, *Physical Fluid Dynamics* (England: Van Nostrand Reinhold), Chap. 3.

Tsinganos, K. C. 1980, *Ap. J.*, **239**, 746.

Unno, W. and Ribes, E. 1976, *Ap. J.*, **208**, 222.

van Ballegooijen, A. A. 1982, *Astron. Astrophys.*, **106**, 43.

Wang, H. 1986, in preparation.

Wilson, P. R. and Simon, G. W. 1983, *Ap. J.*, **273**, 805.

Zirin, H. 1972, *Solar Phys.*, **22**, 34.

Zirin, H. 1985, *Aust. J. Phys.*, **38**, 961.

Zirin, H. 1986, private communication.

Zwaan, C. 1978, *Solar Phys.*, **60**, 213.

TABLE 1

Date	Flux (10^{18}Mx)	V_m (km/s)	V_b (km/s)	V_o (km/s)	Radius (km)	$B_{//}^{mean}$ Gauss	Ini. Sepa. (km)	Mean Sepa. (km)	Arch	Pore	θ_{min} (degree)
04/08/84	694.0	0.28	0.36	5.03	4700	1000	17500	21900	Y	Y	87
06/21/84	198.0	0.75	0.67	3.18	3300	579	17900	22000	Y	Y	77
07/12/83	122.0	0.31	0.57	3.65	2500	621	14200	17200	Y	Y	85
12/17/81	110.0	0.60	0.43	3.30	2500	560	5100	9700	Y	N	80
06/21/84	57.0	0.36	0.33	2.28	2200	375	11400	13600	Y	Y	81
10/14/85	43.0	0.88	0.98	1.72	2200	283	9000	11000	N	N	63
10/14/85	32.0	0.66	0.69	1.28	2200	210	11000	14000	N	N	63
07/12/83	30.0	0.44	0.35	1.88	1800	295	4000	5900	N	N	77
07/21/81	30.0	0.30	0.32	2.45	1600	373	5500	8000	Y	N	83
07/22/85	30.0	0.34	0.51	0.60	3000	106	3700	8500	N	N	60
06/22/85	21.0	0.69	0.64	1.04	2000	167	6500	12000	N	N	56
10/15/85	20.0	0.44	0.49	1.25	1800	196	7500	9700	N	N	71
06/22/85	20.0	0.80	0.85	1.43	1700	220	3500	5400	N	N	61
06/22/85	15.0	0.24	0.38	1.66	1400	244	5500	6400	N	N	82
10/15/85	14.0	0.92	0.74	2.66	1100	368	5000	7000	N	N	71
08/29/84	13.0	0.19	0.17	0.39	2500	66	5000	7500	N	N	64
06/21/84	12.0	0.20	0.46	1.87	1200	265	4800	8100	N	-	84
07/12/83	11.0	1.07	1.18	1.72	1200	243	2200	3400	N	N	58
10/15/85	10.0	0.83	1.05	1.56	1200	221	4000	9200	N	N	62
10/15/85	8.0	0.88	0.52	1.05	1300	151	5000	7800	N	N	50
06/21/84	7.9	0.55	0.39	1.50	1100	208	6000	8300	N	-	70
10/15/85	7.2	0.61	0.59	0.51	1700	79	5500	9200	N	N	40
06/22/85	5.5	0.49	0.64	1.29	1000	175	4000	5300	N	N	69
06/22/85	3.3	0.98	0.81	2.46	600	292	5500	7400	N	N	68

FIGURE CAPTIONS

FIG 1.—(a) Separation of opposite poles *versus* time for the nineteenth bipole in Table 1. The error is about 1000 km. The straight line is a least-square linear fit of the steepest portion of the curve, which is chosen by eye.

FIG 1.—(b) Magnetic flux of two poles *versus* time for the nineteenth bipole in Table 1.

FIG 2.—(a) Same as Figure 1a, but for the sixth bipole in Table 1. The variation in the beginning is caused by the uncertainty in defining the position of the emerging flux at the very early stage.

FIG 2.—(b) Same as Figure 1b, but for the sixth bipole in Table 1.

FIG 3.—Separation velocity of borders, v_b, *versus* separation velocity of maxima, v_m.

FIG 4.—separation velocity of maxima, v_m, *versus* magnetic flux.

FIG 5.—separation velocity of maxima, v_m, *versus* line-of-sight component of mean magnetic field, $B_{//}^{(mean)}$.

FIG 6.—Temperature difference, ΔT, as a function of depth below the photosphere, calculated from Spruit's convection zone model. The initial position is set at a depth of 5000 km.

FIG 7.—Measured separation velocity, v_m, *versus* v_o, which is $B_{//}^{(mean)}\, a^{-1/4}$.

FIG 8.—Minimum elevation angle, θ_{min}, *versus* mean separation.

FIG 9.—Schematic picture of a flux tube at the photosphere. The lower part is a close view of a segment near the surface. The flux tube moves from (from $\overline{DE}$ to $\overline{GH}$) as it rises. The apparent displacement of the tube at the photosphere is AB, which is equal to $CB/sin\theta$.

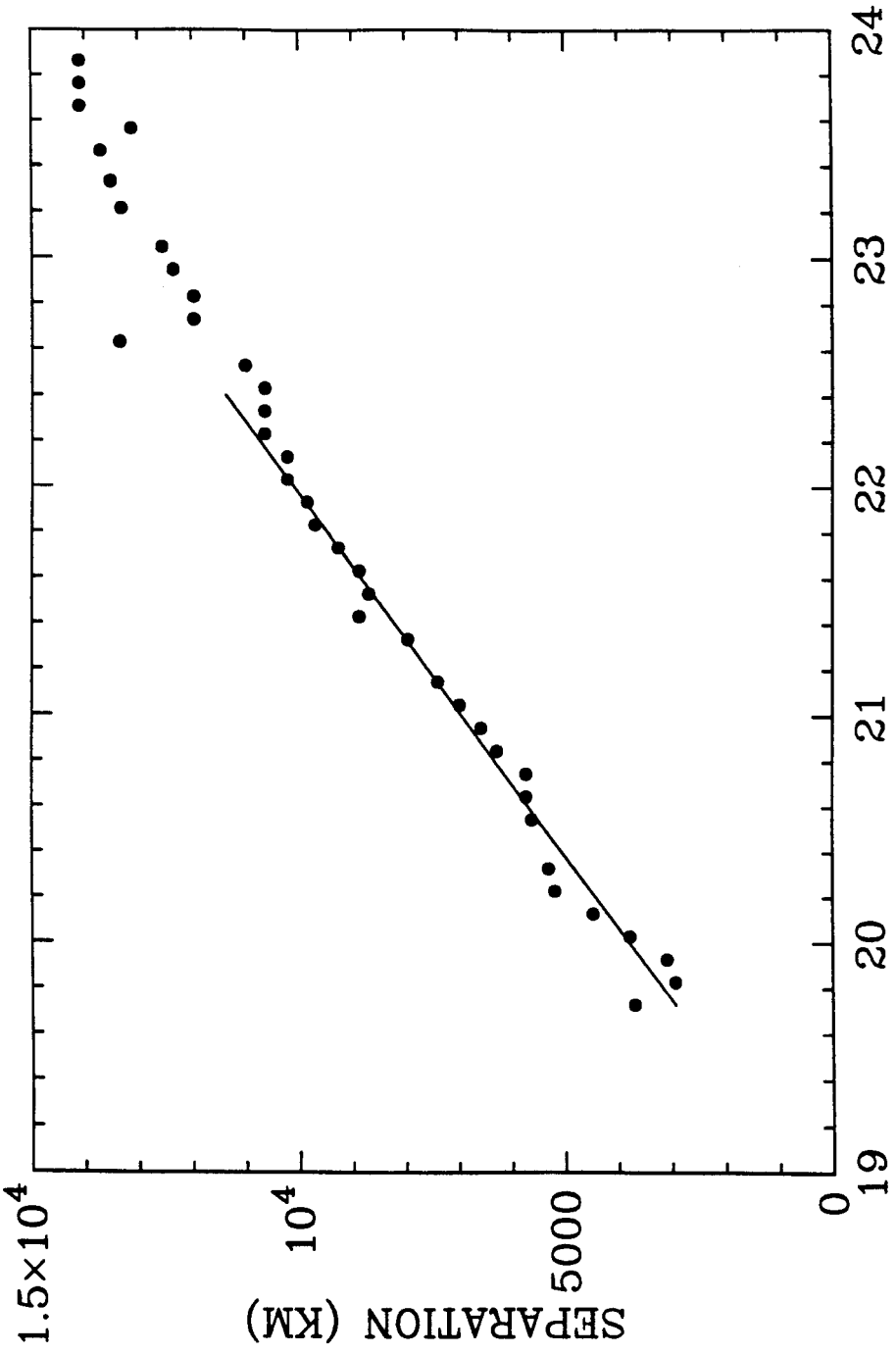

FIGURE 1a

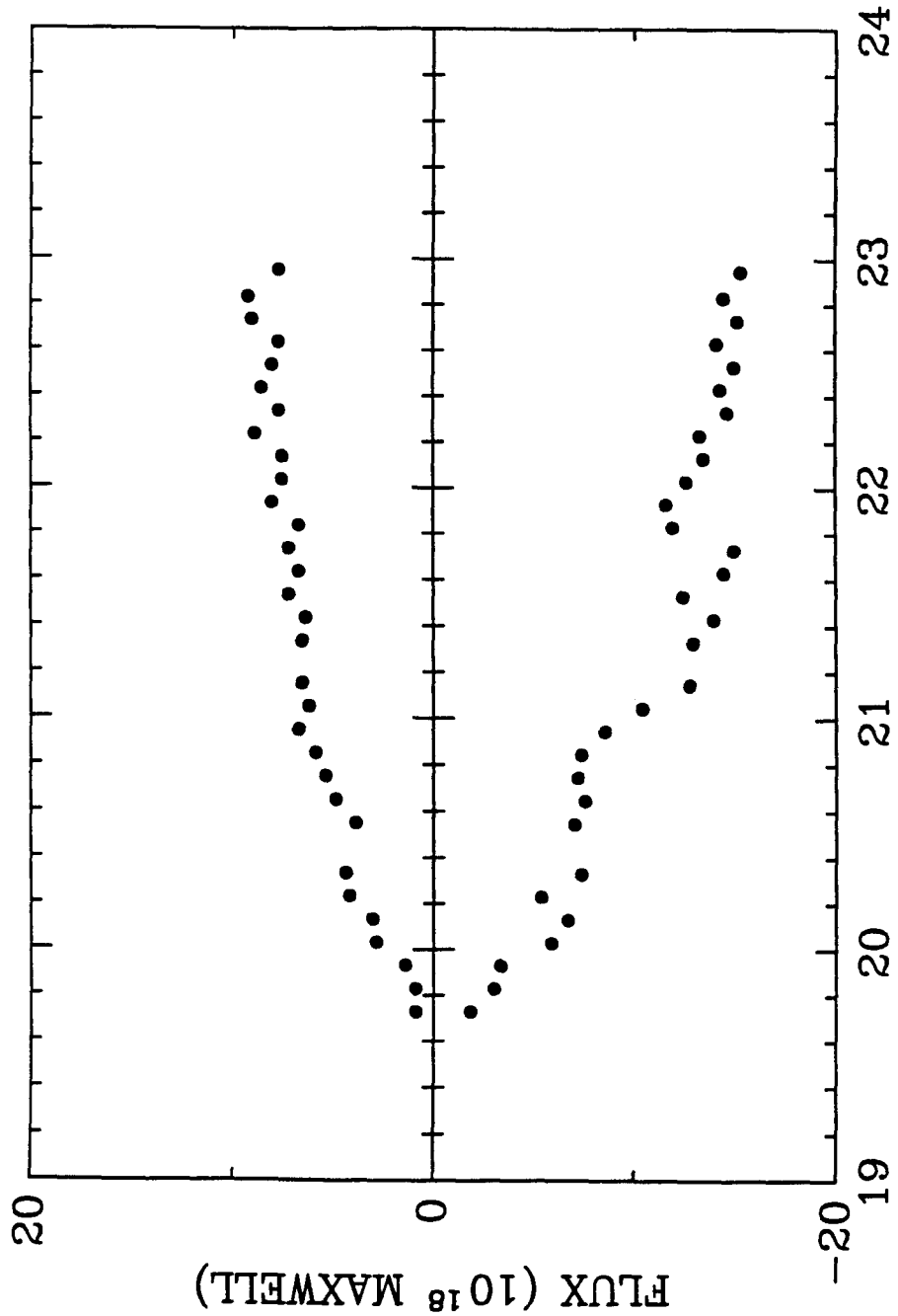

FIGURE 1b

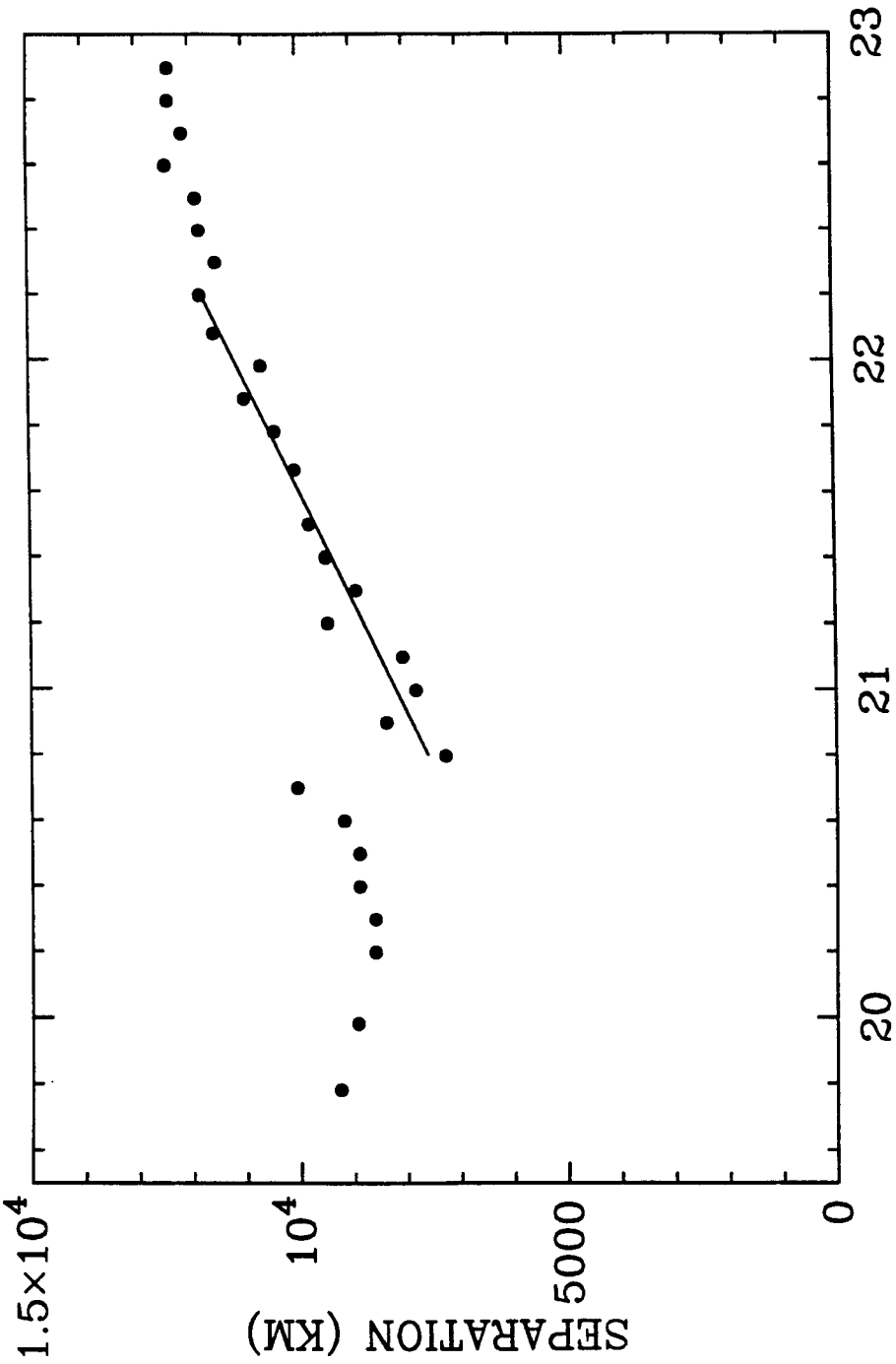

FIGURE 2a

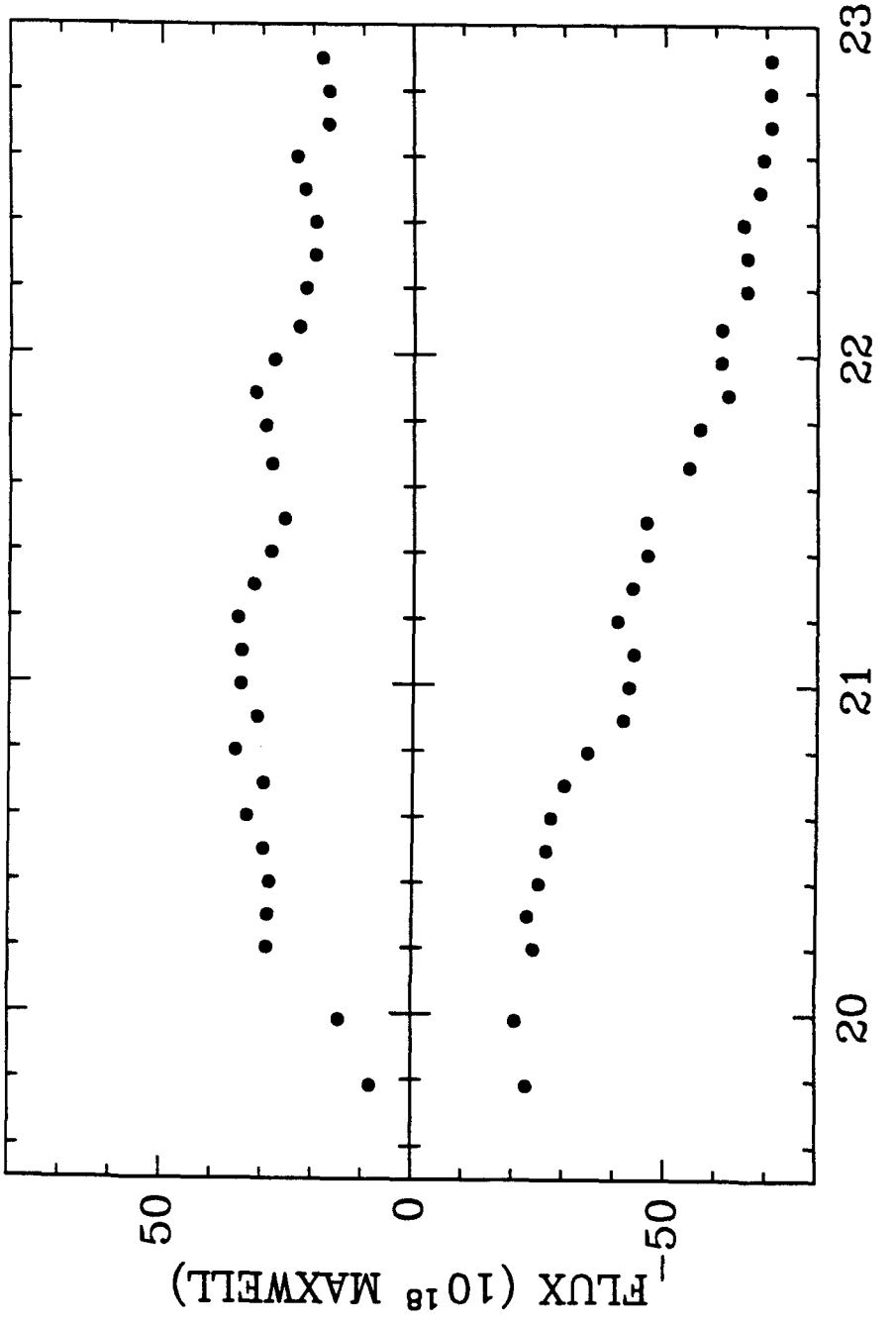

FIGURE 2b

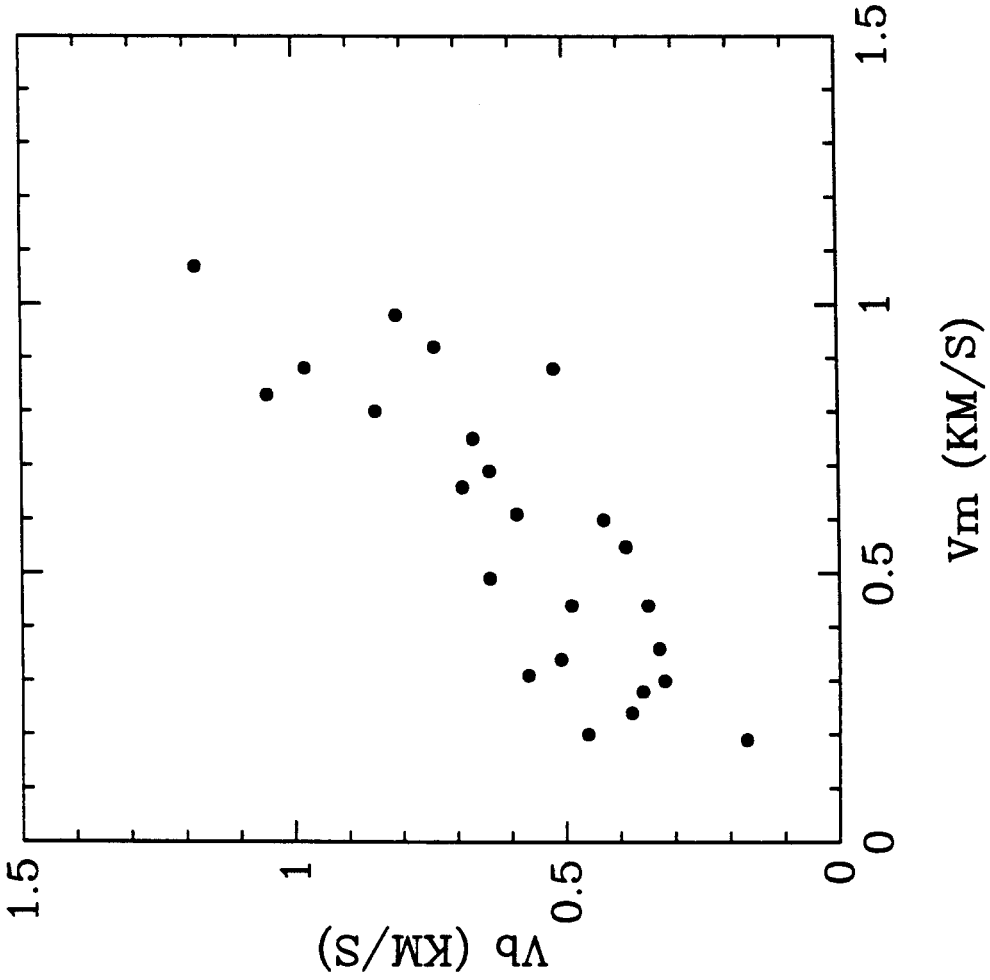

FIGURE 3

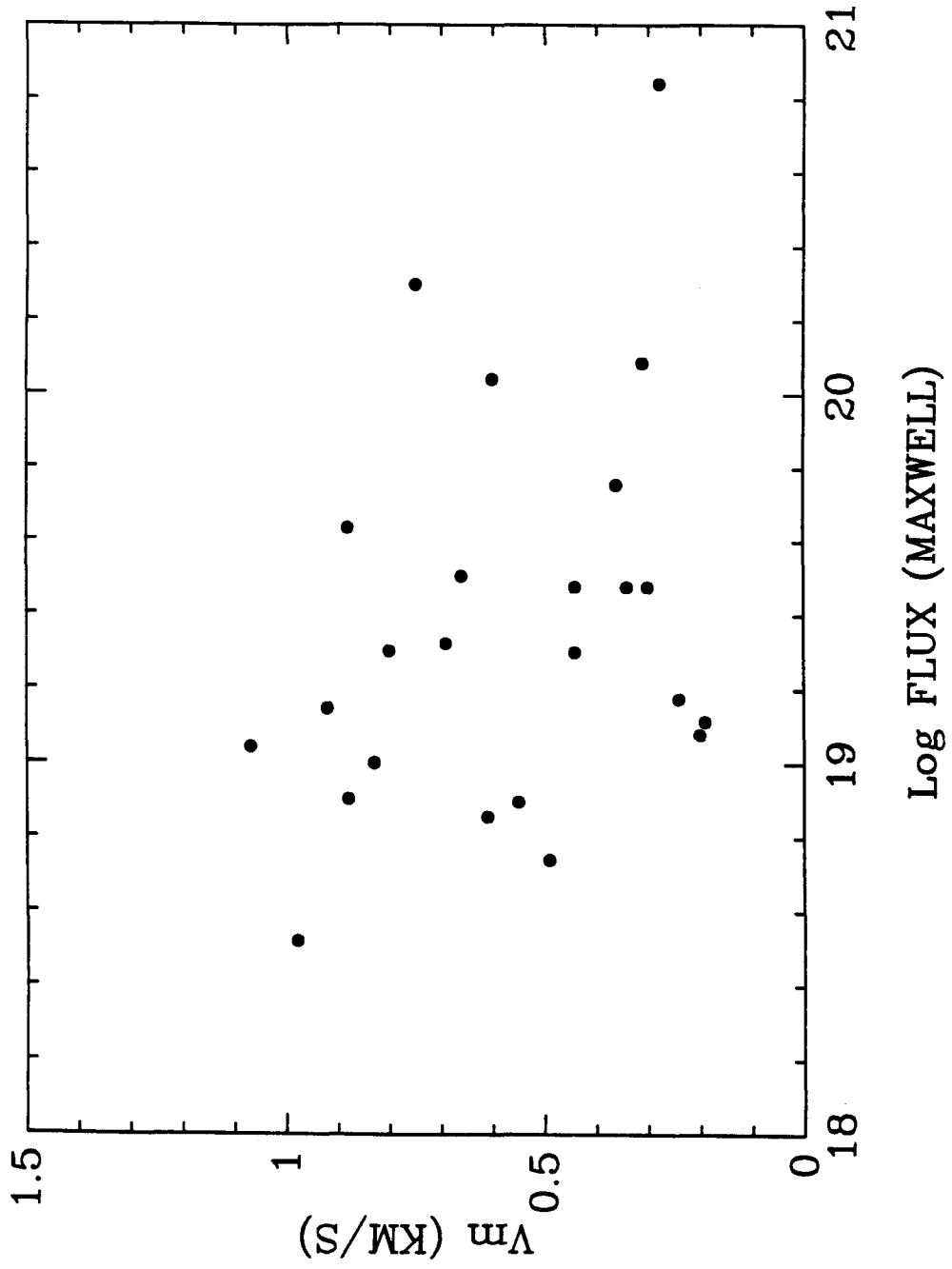

FIGURE 4

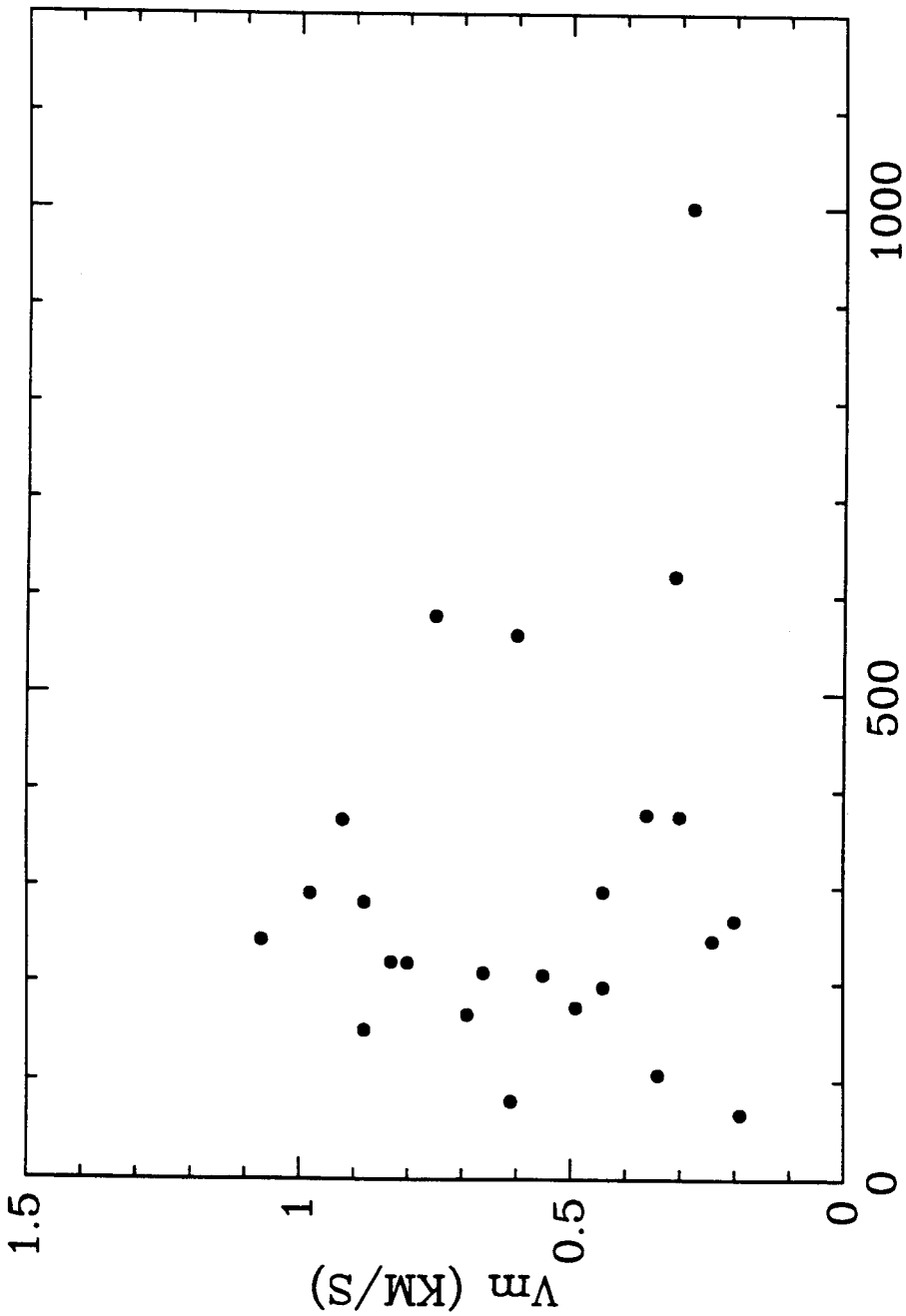

FIGURE 5

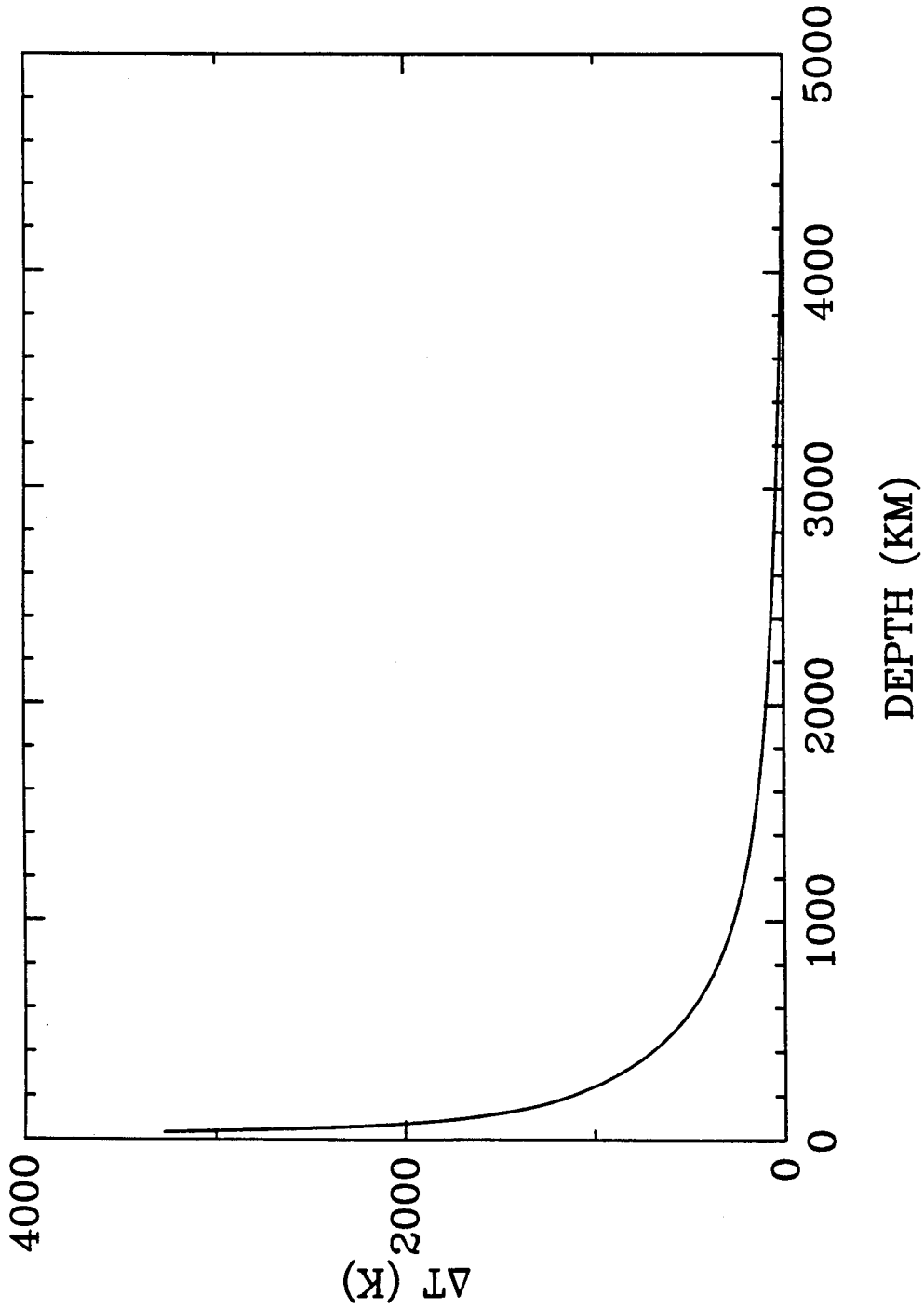

FIGURE 6

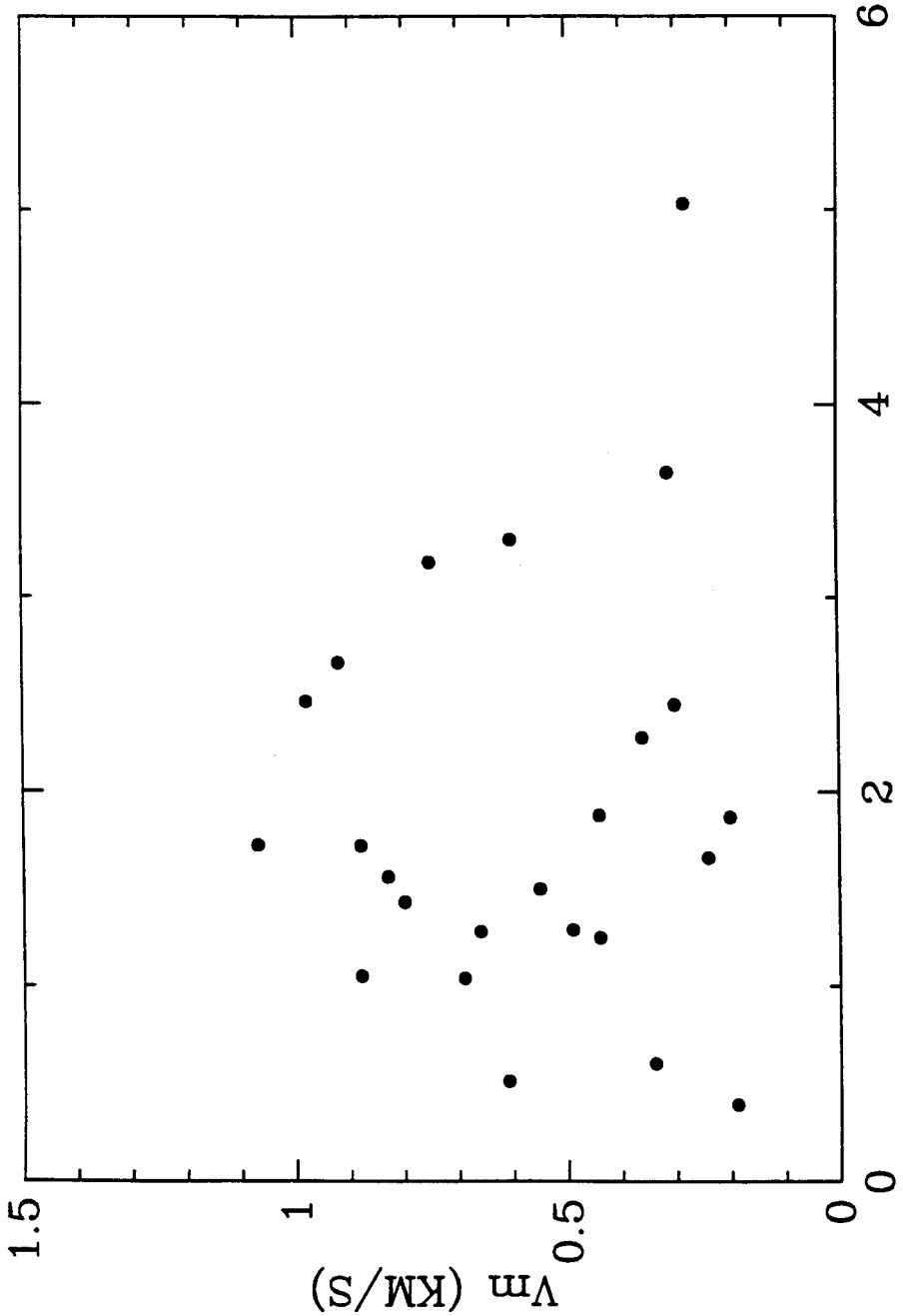

FIGURE 7

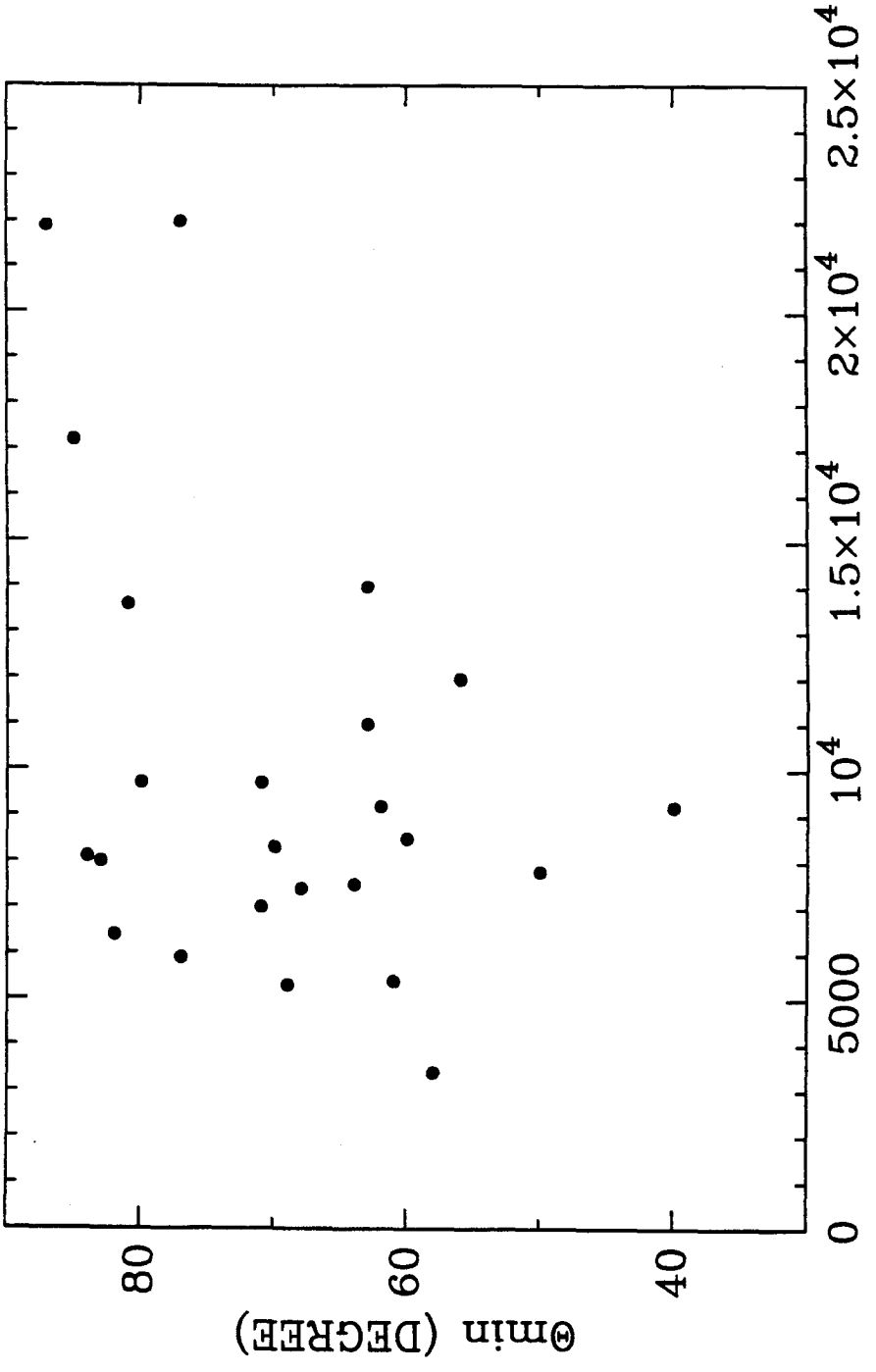
80
60
40
θmin (DEGREE)
0
5000
10^4
1.5×10^4
2×10^4
2.5×10^4
MEAN SEPARATION (KM)

FIGURE 8

FIGURE 9

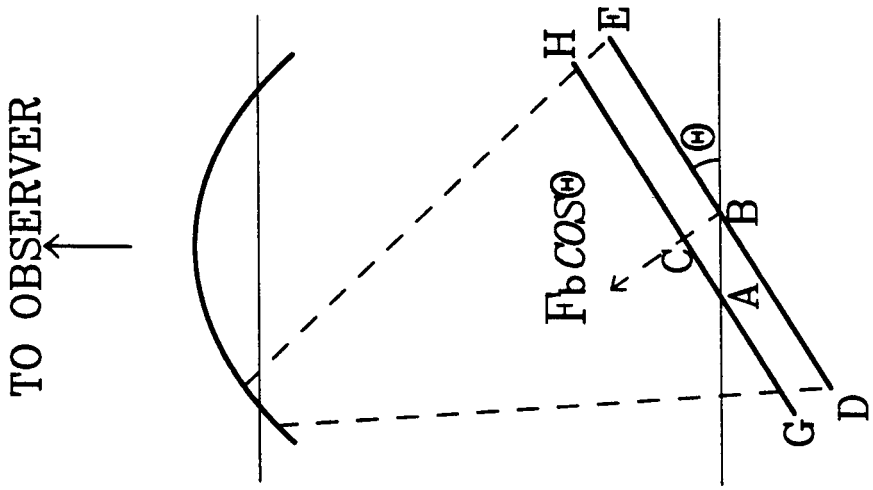

CHAPTER 3

THE COOLING TIME SCALES OF GROWING SUNSPOTS

To be published in The Astrophysical Journal

Volume 312, 1987

ABSTRACT

We study the evolution of brightness and magnetic fields of growing sunspots. Growing sunspots are found to be brighter (or less dark) than stable sunspots with the same magnetic field strength. From comparison of brightness and magnetic fields of a growing sunspot with those of stable sunspots, we obtain a dynamical parameter, the cooling time, of the growing sunspot. Ten growing sunspots are studied, and cooling times of 0.5 to 9 hr are found. Two models, the *Inhibition Model* and the *Alfvén Wave Model*, give cooling times of about 0.05 hr, based on linear theory. The discrepancy between theory and observation may be due to the fact that the observed sunspots are in the nonlinear regime.

I. INTRODUCTION

The low temperatures and strong magnetic fields of sunspots constitutes one of the oldest problems in solar physics. Two models, the *Inhibition Model* and the *Alfvén Wave Model*, have been proposed to explain the darkness of sunspots. In the *Inhibition Model*, first proposed by Biermann (1941), the convection which carries energy up to the photosphere is partially inhibited by magnetic fields. In the *Alfvén Wave Model*, thermal energy is transformed into mechanical energy. In the presence of magnetic fields, under certain circumstances, a temperature gradient can cause overstable modes of Alfvén waves (or more complicated magnetoacoustic waves) which can carry a large amount of energy away (Chandrasekhar 1961; Danielson 1965; Savage 1969; Parker 1974a,b, 1975; Cowling 1976a). The criterion for occurrence of overstability is that the thermal conductivity be greater than the magnetic diffusivity. On the Sun, this criterion is satisfied at a depth of less than 2000 km (Meyer et al. 1974).

Several authors have provided much theoretical and observational evidence for or against these two models (Danielson 1965; Savage 1969; Moore 1973; Parker 1974a,b, 1975, 1977; Cowling 1976a,b; Roberts 1976; Beckers 1976; Beckers and Schneeberger 1977; Boruta 1977; Thomas 1978; Galloway and Moore 1979; Galloway and Weiss 1981; Spruit 1978,1981). Most of this work, however, is time independent. In this paper, a method is proposed to provide *dynamical information* which is the cooling time scale of growing sunspots.

In these two models, the intensity of a sunspot should depend only on the magnetic structure and field strength in the equilibrium state. If the mechanism to reduce the intensity of a sunspot operates only in a shallow region, for sunspots above a minimum size, the intensity of a growing sunspot should be a function only of its observed photospheric field strength. This dependence can be determined by

observing the intensities and magnetic fields of stable sunspots which have already reached their equilibrium states. This means that a unique *I versus B* (intensity *versus* field strength) curve can be obtained from observations.

During the transition period before a sunspot reaches an equilibrium state, growing sunspots have higher intensities than stable sunspots with the same magnetic field strength. As the sunspot cools, the intensity decreases and the magnetic field increases as both approach the equilibrium values, which lie on the *I versus B* curve obtained from the stable sunspots. Therefore we expect that, in the I - B plane, the track of a growing sunspot will be located above the *I versus B* curve of the stable sunspots. The cooling time of a growing sunspot is obtained from the rate of approach of its track to the *I versus B* curve of the stable sunspots.

II. OBSERVATIONS AND DATA ANALYSIS

The digital magnetograms of the line-of-sight component of solar magnetic fields are made with a videomagnetograph at the Big Bear Solar Observatory (BBSO). The videomagnetograph at BBSO has been discussed by Martin (1983) and Zirin (1985). The calibration of magnetic fields is done by the standard method of BBSO. The line-of-sight component of the magnetic field of a sunspot is measured by averaging over 3 by 3 pixels at the center of the sunspot. The scale is approximately one-half arcsecond per pixel. It is assumed that the magnetic field at the center of a sunspot is perpendicular to the surface of the Sun, so that the line-of-sight component can be transformed into the magnetic field strength.

The intensity is observed in the Ca I line (6103 Å) with an effective bandpass of 0.5 Å(FWHM) for convenience because the magnetic field is observed at this wavelength. The FWHM of this Ca I line is about 0.15 Å. Because the bandpass is much larger than the line width, it is a good approximation that the observed

intensity in the line is proportional to the intensity of the continuum. Therefore the observed ratio of sunspot to photospheric intensity in the line is equal to that in the continuum. The intensity of a sunspot is also measured by averaging over 3 by 3 pixels at the center of the sunspot. The scattered light at the center of a sunspot is corrected by measuring the intensity outside the limbs (Maltby 1971). A different correction is applied to each sunspot according to its size. The correction is about 0.14 I_o, if the diameter of the sunspot is 1500 km and the observed intensity is 0.7 I_o; 0.06 I_o, if the diameter is 7000 km and the observed intensity is 0.3 I_o, where I_o is the photospheric intensity.

a) Stable Sunspots

We define a stable sunspot as one that has lived at least one day and whose magnetic field and intensity do not change significantly during the observing time. It may be a very slowly decaying sunspot.

We have studied fifteen stable sunspots. Their magnetic fields and intensities are plotted in Figure 1. Some sunspots have more than one point in the $I - B$ plane because they were observed at different times. The error bars in Figure 1 indicate only the random errors in the intensity and field strength measurements. The random and systematic errors due to the correction of stray light are not included.

Figure 1 shows that all stable sunspots fall within a narrow belt in the $I - B$ plane. Therefore, it is reasonable to assume that the intensity of a stable sunspot is determined only by its magnetic field strength. A third-order polynomial curve which fits the data is used to represent the relationship between the intensity and the magnetic field.

From Figure 1, the I *versus* B curve is not very dependent on the size of

sunspots. Therefore, we use one curve for all stable sunspots.

b) Growing Sunspots

Ten growing sunspots in emerging flux regions and active regions have been studied. Their intensities and magnetic fields are shown in Figure 2. Compared with the stable sunspots, the growing sunspots have significantly higher intensities for *the same magnetic field.* Two typical growing sunspots (numbers 1 and 8) are shown in Figure 3. Their magnetic fields *versus* time are shown in Figure 4. The track of a growing sunspot in the $I - B$ plane approaches the I *versus* B curve of the stable sunspots. This suggests that a new sunspot requires time to cool down and reach the equilibrium state. The cooling time is calculated in section III.

It is important to determine whether the growing sunspots reach the curve of the stable sunspots. Unfortunately, a few hours' observation is usually not long enough to observe this happen, and the growing sunspots are very difficult to identify the next day. Only one spot (number 9) can be identified easily the next day. It does reach the curve of the stable sunspots. This is shown in Figure 3.

III. COOLING TIME SCALES

Since the brightness of growing sunspots is higher than those of stable sunspots with a given magnetic field, it takes time for the growing sunspots to cool down and reach the equilibrium state. The cooling time scale of interest is the time scale which a sunspot takes to reach the equilibrium state *at a fixed magnetic field strength* . If constant magnetic fields are turned on in a certain region, what is the time scale for the system to cool down and reach the equilibrium state? We define this cooling time τ as:

$$\frac{1}{\tau} = -\frac{\partial \ln(I_g - I_s)}{\partial t}\bigg|_B, \qquad (1)$$

where I_g is the intensity of a growing spot and I_s the intensity of a stable spot. As it grows, the magnetic field of the sunspot also increases. The increase might be due to either the external forces or feedback from the cooling of the sunspot. The apparent change of $\ln(I_g - I_s)$ can be split into two terms:

$$\frac{d \ln(I_g - I_s)}{dt} = \frac{\partial \ln(I_g - I_s)}{\partial t}\Big|_B + \frac{\partial \ln(I_g - I_s)}{\partial B}\Big|_t \cdot \frac{\partial B}{\partial t}. \qquad (2)$$

The apparent change, $d \ln(I_g - I_s)/dt$, can be obtained from the track of the growing sunspot and the curve of the stable sunspots in the $I - B$ plane. Since $\partial I_g(B)/\partial B|_t = 0$,

$$\frac{\partial \ln(I_g - I_s)}{\partial B}\Big|_t = \frac{-\partial I_s(B)/\partial B|_t}{(I_g - I_s)}. \qquad (3)$$

We obtain $\partial I_s(B)/\partial B|_t$ from the curve of the stable sunspots. Observations also provide $\partial B(t)/\partial t$.

Therefore, the cooling time scale of a growing sunspot can be determined purely from observation. The cooling time is a function of the magnetic field strength. The plot of the cooling time *versus* magnetic field is shown in Figure 5 for spots 1 and 8. If we assume that the B–dependence of the cooling time can be approximated by a power law

$$\tau \propto B^{\alpha}, \qquad (4)$$

for each growing sunspot, the index, α, can be determined. For each of the ten growing sunspots, the index, α, and the cooling time scales are listed in Table 1. The average of α over ten growing sunspots is -0.9 ± 0.4. However, note from Table 1 that there appears to be little dependence of τ on the value of B averaged over different sunspots. But difficulties in comparing directly different sunspots should be noticed.

IV. ESTIMATIONS OF COOLING TIME SCALES FROM MODELS

a) The Inhibition Model

According to this model, the convection which carries thermal energy upward is partially inhibited by magnetic fields. The time scale for the convection to be stopped (or reduced) is of the order of the turnover time of a convection cell (Galloway and Moore 1979; Galloway and Weiss 1981). The size of convection cells is of the order of scale height, which implies $\tau \simeq \epsilon_1 \cdot H/v$, where H is the pressure scale height, v is the velocity of the convection and $\epsilon_1 \simeq o(1)$. Therefore, H/v is depth dependent. The value relevant to the cooling time is the smallest one, because if the convection is stopped in one layer then energy can no longer be transported. The quantity, H/v, is calculated by using Spruit's data (1974) and is plotted in Figure 6. The minimum of H/v which occurs at a depth of 50 km is about 0.05 hr. When the energy transport is stopped in this layer, the remainder of energy above this layer is carried away by radiation in a time scale l^2/κ, where κ, the thermal diffusivity, is about $3 \times 10^{12} cm^2/sec$ (Meyer et al. 1974). If l is taken to be 50 km, then $l^2/\kappa \simeq 0.002$ hr, which is much shorter than the minimum turnover time of 0.05 hr. Therefore we adopt 0.05 hr as the predicted cooling time. The coefficient, ϵ_1, might decrease as the magnetic field increases, but the exact dependence is unknown. This needs further investigation in order to make comparisons with the observations.

b) The Alfvén Wave Model

If the thermal conductivity is greater than the magnetic diffusivity, the temperature gradient can cause overstable modes (Chandrasekhar 1961; Danielson 1965; Savage 1969; Moore 1973; Parker 1974b; Roberts 1976; Cowling 1976a). The

amplitudes of these modes can increase exponentially in the linear regime, then settle down to the stable value in the nonlinear regime by nonlinear processes. The energy flux transported by these modes is $J = \frac{1}{2}\rho v^2 V_A$. v is the amplitude of the Alfvén wave and V_A is the Alfvén speed. If v is significantly large, these modes can carry a lot of energy. If 80% of the photospheric energy is transported by Alfvén waves, $v \simeq 8\,km/sec$ is required for $B = 1000\,G$. The cooling time scale is

$$\tau \simeq -\epsilon_2 \cdot \left(\frac{d \ln J}{dt}\right)^{-1} \simeq -\frac{1}{2}\epsilon_2 \cdot \left(\frac{d \ln v}{dt}\right)^{-1} \simeq \frac{1}{2}\epsilon_2 \tau_v \qquad (5)$$

where τ_v is the $e-folding$ time of the amplitude of the velocity of the overstable mode. From work of other authors (Roberts 1976), $\tau_v \simeq d/V_A$, where d is the vertical scale of the system in which the thermal conductivity is greater than the magnetic diffusivity. From Meyer et al. (1974), $d \simeq 2000\,km$. The Alfvén speed $V_A = B/\sqrt{4\pi\rho}$ is roughly constant with depth if the temperature deficit is small. For $B(z=0) = 1000\,G$ and $\rho(z=0) = 3.2 \times 10^{-7}\,g/cm^3$, $V_A = 5\,km/sec$. If $\epsilon_2 = 1$, then $\tau = 0.06\ hr$. Since $V_A \propto B$, we find $\tau \propto B^{-1}$, and therefore $\alpha = -1$.

Both the *Inhibition Model* and the *Alfvén Wave Model* give $\tau \simeq 0.05\,hr$. This is about two orders of magnitude lower than the observed value. But one must bear in mind that the estimates are based on the linear theory, while the observations are beyond the linear regime, because the intensity deficit is usually greater than 0.1. We can see this as follows: for the *Alfvén Wave Model*, if $I/I_o \simeq 0.9$, an oscillation amplitude of $v \simeq 3\,km/sec$ is required. Then $\delta B/B \simeq v/V_A \simeq 3/5 \simeq 0.6$, if $B = 1000\ G$. This is well beyond the linear regime. Therefore ϵ_1 and ϵ_2 might be greater than $o(1)$.

V. DISCUSSION

a) Comparison of the I versus B Curve with Results of Others

The relationship between the intensity and the magnetic field has been given by other authors (Bray and Loughhead 1964, Deinzer 1965, Dicke 1970). It is shown in Figure 7, where T and T_o are effective temperatures of a sunspot and of the photosphere, respectively. In their papers, it is not mentioned whether all sunspots are stable or not. Presumably all sunspots they observed are stable. To compare our results with these, we have transformed I(6103 Å) into effective temperature T by assuming there is LTE:

$$\frac{I}{I_o} = \frac{e^{hc/\lambda KT_o} - 1}{e^{hc/\lambda KT} - 1} \tag{6}$$

where $T_o = 5800$ K and $\lambda = 6103$ Å. The Bray and Loughhead data are indirectly derived from *temperature versus umbral size* and *magnetic field versus umbral size.*

We see in Figure 7 that the T *versus* B curve has roughly the same slope but T varies by 30% among the different authors. Our result is in the middle. The discrepancies of the T *versus* B diagram among various authors might be caused by different calibrations of magnetic fields and different corrections for stray light. Differences in observed wavelengths might also contribute the discrepancies because layers of various depth are observed. Despite the difference, the data of each author fall within a narrow belt. Therefore it is reasonable to use a unique I *versus* B relation for all stable sunspots.

b) Comparisons of Intensities of Growing Sunspots and Stable Sunspots

Our data on the growing and stable sunspots are observed with the same system. Magnetic fields are calibrated by the same method and stray light is also corrected in the same way. Even if the calibrations and stray light corrections might

not be accurate, the results are consistent. The measured magnetic field strength in some of our sunspots is less than 1000 Gauss. Those measurements agree well with those at KPNO (Table 2) for the same sunspots. It is widely held (Beckers 1981; Zwaan 1981; Zwaan and Brants 1981), but not proven, that all sunspots have field strength greater than 1000 Gauss. Whether this is true or not does not affect our argument, since we compare sunspots of the same measured field strengths. Whatever the ratio of true to observed fields may be, one must map into the other, that is, our observed relative field strengths form a consistent sequence; and it is the relative field strength that matters in this paper. If all sunspots are indeed stronger than 1000 Gauss, then the positions of sunspots in Figure 1 and Figure 2 would simply be shifted to the right; each observed value would correspond to some "true" value. It should be pointed out that, for the sunspots of the same size, the effect of stray light should be the same. Our observations show that, *for the sunspots of similar size*, the growing sunspots are brighter than the stable sunspots of *the same observed magnetic field strength*. This is independent of the value of that field strength. Therefore, the result that the growing sunspots have higher intensities than the stable sunspots *for the same magnetic field strength* is convincing.

Because a larger stray light correction would increase the field strength and decrease the brightness for both the growing sunspots and the stable sunspots, the curve of the stable sunspots in Figure 1 and the tracks of the growing sunspots in Figure 3 would not change much and the derived cooling time scales of the growing sunspots would be only slightly changed. The growing sunspots start out brighter than the stable sunspots, then march toward the curve of the stable sunspots, while the stable sunspots stay on the curve for a long period, although they might move from one point to another point along it.

c) Cooling Time Scales

The cooling time scale is defined as the rate of change of the intensity *at a fixed magnetic field strength*. Therefore it is independent of the mechanism which causes increases of magnetic fields, and it is also independent of whether a sunspot consists of a number of unresolved flux tubes or not. The cooling times of the ten sunspots studied range from 0.5 to 9 hr. There is no apparent correlation between the cooling time and the umbral size for the same magnetic field, nor is there one for the index α and the size.

We have shown, from the linear theory, that both models give a similar cooling time $\tau \simeq 0.05$ hr which is far shorter than the observed value. The discrepancy between theory and observation may be due to the fact that the observed sunspots are in the nonlinear regime. For the *Alfvén Wave Model*, the nonlinear interaction could restrict the growth of overstable modes. This causes the time scale of growth to be longer than that of the linear theory. For the *Inhibition Model*, the convective speed is decreasing. Therefore the turnover time might increase significantly. This leads to the cooling time being longer than that estimated above.

The measured index α usually has a large error because of the errors in the cooling time and the field strength. The standard deviation in Table 1 includes only the random errors in the intensity and field strength measurements. If the random and systematic errors due to the undercorrection of stray light are taken into account, the index α could have a larger error and the value of $|\alpha|$ could be larger. The range of the measured α is from -5.0 to $+0.2$. The mean of -0.9 ± 0.4 is close to -1, which is estimated from the *Alfvén Wave Model* by assuming the overstable modes are pure Alfvén Waves. In a real situation, the overstable modes are the more complicated magnetoacoustic waves since the Alfvén speed is comparable to the sound speed. The time scale τ_v in equation (3) might

not be simply proportional to V_A^{-1}. This means that α is not simply equal to -1. More realistic theoretical work on the *Alfvén Wave Model* is needed to determine $\tau(B)$.

In the *Inhibition Model*, stronger magnetic fields should inhibit convection more quickly. This means that α is negative. But the exact dependence of τ on B is difficult to understand.

The difference between observed and predicted cooling times is so large that it cannot be due to observational error, nor can it be used to distinguish models, because they have nearly the same cooling time. Rather, the model calculations need to be improved. Numerical model simulations which extend to the nonlinear regime should give more realistic results.

d) Significance of I versus B Diagram

Since the anomalous intensity of magnetic features on the Sun is usually caused by magnetic fields, the *I versus B* diagram can provide a lot of information on magnetic features. For example, the distribution of sunspots and faculae in the I - B plane could help us to understand the mechanisms which cause these anomalous intensities. The evolution of individual features in the I - B plane could give *dynamical information*, as we have applied here to sunspots.

VI. SUMMARY

(1) We found that growing sunspots are brighter than stable sunspots with the same magnetic field strength.

(2) We defined and calculated cooling times of ten growing sunspots. They range from 0.5 to 9 hr.

(3) The average of index α of the power law, $\tau \propto B^{\alpha}$, over ten growing sunspots,

is -0.9 ± 0.4. However, the cooling time, τ, is little dependent on the value of B averaged over different sunspots.

(4) We estimated the cooling time τ and index α from two models based on linear theory. Both models give $\tau \simeq 0.05\, hr$. The *Alfvén Model* gives $\alpha \simeq -1$.

(5) The discrepancy between theoretical and observed cooling times may be due to the fact that the observed sunspots are in the nonlinear regime.

REFERENCES

Beckers, J. M. 1976, *Ap. J.*, **203**, 739.

Beckers, J. M., and Schneeberger, T. J. 1977, *Ap. J.*, **215**, 356.

Beckers, J. M. 1981, in *The Sun as a Star*, ed. S. Jordan (NASA SP-450), p. 11.

Biermann, L. 1941, *Vierteljahrsschr. Astr. Gesellsch.*, **76**, 194.

Boruta, N. 1977, *Ap. J.*, **215**, 364.

Bray, R. J., and Loughhead, R. E. 1964, *Sunspots* (New York: Dover) .

Chandrasekhar, S. 1961, *Hydrodynamic and Hydromagnetic Stability*, Chap. 4 (New York: Dover).

Cowling, T. G. 1976a, *Magnetohydrodynamics* (Bristol: Adam Hilger) .

Cowling, T. G. 1976b, *M.N.R.A.S.*, **177**, 409.

Danielson, R. E. 1965, in *IAU Symposium* **22**, *Stellar and Solar Magnetic Fields*, ed. R. Lüst (New York: John Wiley), p. 314.

Deinzer, W. 1965, *Ap. J.*, **141**, 548.

Dicke, R. H. 1970, *Ap. J.*, **159**, 25.

Galloway, D. J., and Moore, D. R. 1979, *Geophys. Astrophys. Fluid Dynamics*, **12**, 73.

Galloway, D. J., and Weiss, N. O. 1981, *Ap. J*, **243**, 945.

Maltby, P. 1971, *Solar Phys.*, **18**, 3.

Martin, S. F. 1983, in *Sacramento Peak Workshop on Small Scale Dynamical Processes* (Sunspot, NM: Sacramento Peak Observatory), p. 30.

Meyer, F., Schmidt, H. U., Weiss, N. O., and Wilson, P. R. 1974, *M.N.R.A.S.*, **169**, 35.

Moore, R. L. 1973, *Solar Phys.*, **30**, 403.

Parker, E. N. 1974a, *Solar Phys.*, **36**, 249.

Parker, E. N. 1974b, *Solar Phys.*, **37**, 127.

Parker, E. N. 1975, *Solar Phys.*, **40**, 275.

Parker, E. N. 1977, *M.N.R.A.S.*, **179**, 93P.

Roberts, B. 1976, *Ap. J.*, **204**, 268.

Savage, B. D. 1969, *Ap. J.*, **156**, 707.

Spruit, H. C. 1974, *Solar Phys.*, **34**, 277.

Spruit, H. C. 1978, *Solar Phys.*, **55**, 3.

Spruit, H. C. 1981, *Space Science Reviews*, **28**, 435.

Thomas, J. M. 1978, *Ap. J.*, **225**, 275.

Zirin, H. 1985, *Aust. J. Phys.*, **38**, 961.

Zwaan, C. 1981, *The Sun as a Star*, ed. S. Jordan (NASA SP-450), p. 163.

Zwaan, C., and Brants, J. J. 1981, in *The Physics of Sunspots*, ed. L. E. Cram and J. H. Thomas (Sunspot, NM: Sacramento Peak Observatory), p. 210.

TABLE 1

COOLING TIMES OF GROWING SUNSOPTS

Spot No.	Time (UT)	Size (km)	α	τ (hr)													
				200 (Gauss)	300	400	500	600	700	800	900	1000	1100	1200	1300	1400	1500
1	18:00-21:44	3700-4800	-5.0 ± 1.9	...	...	...	...	...	...	...	...	...	8.33	6.20	4.35	2.77	1.46
2	18:00-21:10	3700-4800	-1.4 ± 2.3	...	...	...	...	1.04	0.89	0.73	...	...	...	...	...	...	...
3	18:00-21:10	400-3400	-1.4 ± 0.9	...	...	...	...	...	3.68	3.50	3.25	2.91	2.14	1.71	...	...	...
4	18:00-21:10	2200-5200	-2.2 ± 1.4	...	...	...	...	...	4.03	3.27	2.62	2.06	1.57	...	...	...	...
5	18:00-21:10	0-1900	-1.3 ± 1.0	...	1.11	0.84	0.56	...	...	...	...	...	...	...	...	...	...
6	18:00-21:10	0-0	$+0.2\pm0.6$	5.35	5.81	6.25	6.65	...	...	...	...	...	...	...	...	...	...
7	18:00-21:10	400-3000	-0.1 ± 1.0	...	...	3.10	3.11	3.09	3.05	2.98	...	...	...	...	...	...	...
8	19:03-22:50	0-3400	-0.5 ± 2.5	...	...	...	...	...	...	...	...	...	7.51	7.26	6.99	6.70	...
9	16:24-22:50	0-2400	-3.1 ± 2.7	...	...	...	...	...	...	...	6.13	4.90	3.66	2.41	...	...	...
10	19:03-22:50	0-1700	-3.3 ± 1.5	...	...	...	...	...	...	4.90	3.32	2.35	...	...	...	...	...

TABLE 2

COMPARISON OF MAGNETIC FIELDS OF SUNSPOTS OF AUGUST 2, 1984

	Time (UT)	B (Gauss)					
Kitt Peak	16:00	684	521	447	612	227	377
BBSO	18:35	827	474	500	732	243	384

FIGURE CAPTIONS

FIG 1.—Intensity of stable sunspots, in units of photospheric intensity, as a function of magnetic field strength. The solid curve is a third-order polynomial fit. The sizes shown in the upper right corner are the diameters of sunspots, within which the intensity is 80% of photospheric intensity.

FIG 2.—Intensity of growing sunspots, in units of photospheric intensity, as a function of magnetic field strength. The curve is the same as in Figure 1.

FIG 3.—Same as Figure 2, but for growing sunspots 1, 8, and 9. The curve is the same as in Figure 1.

FIG 4.—Magnetic field strength *versus* time for growing sunspots 1 and 8.

FIG 5.—Cooling time *versus* magnetic field strength on a logarithmic scale for growing sunspots 1 and 8.

FIG 6.—Ratio of the scale height to the convective speed as a function of depth below the surface of the sun, based on Spruit's model (Spruit 1974).

FIG 7.—Temperature of stable sunspots, in units of photospheric intensity, as a function of magnetic field strength, from various authors.

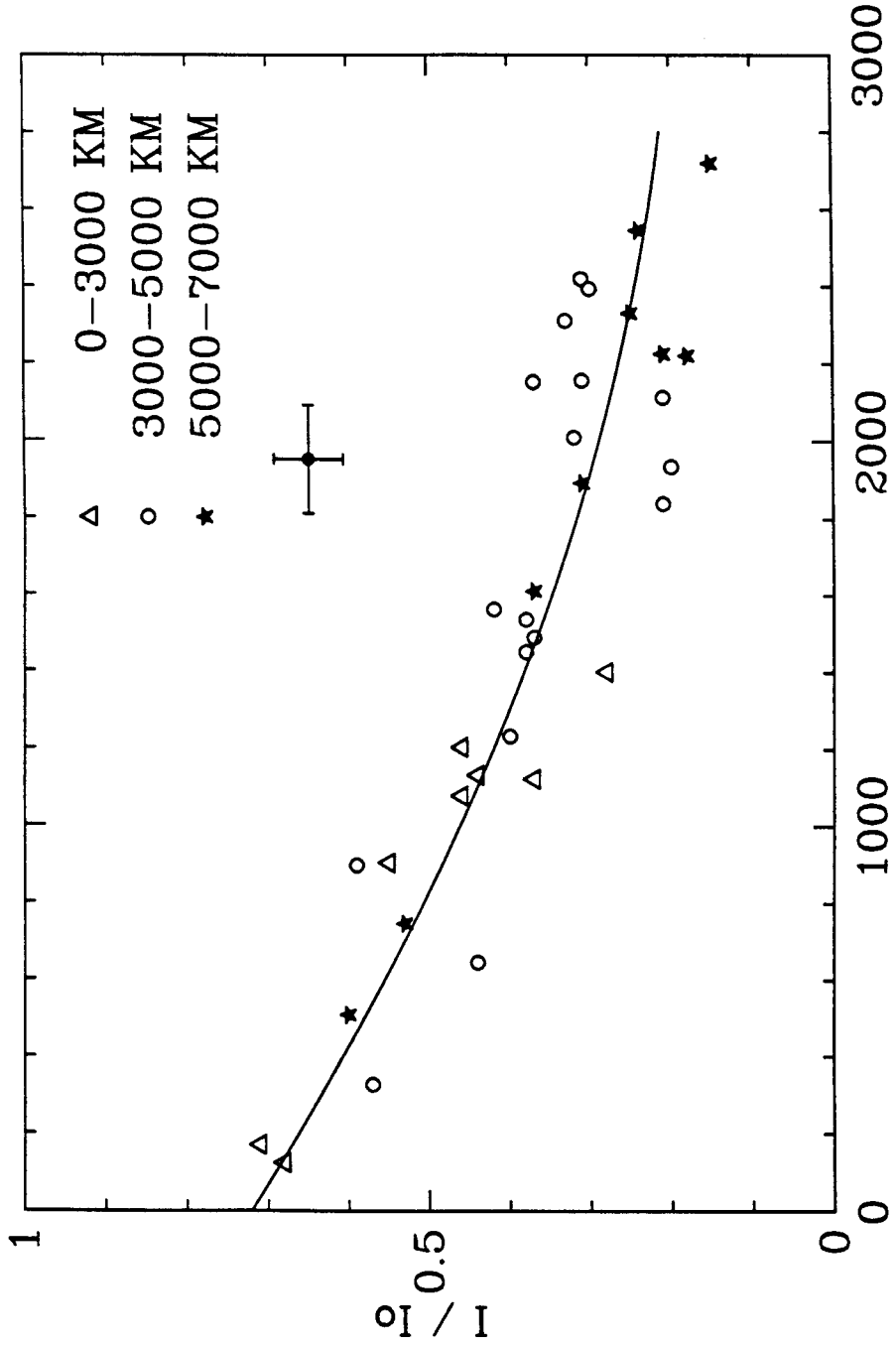
0-3000 KM
3000-5000 KM
5000-7000 KM
I / Io
1
0.5
0
0
1000
2000
3000
B (GAUSS)

FIGURE 1

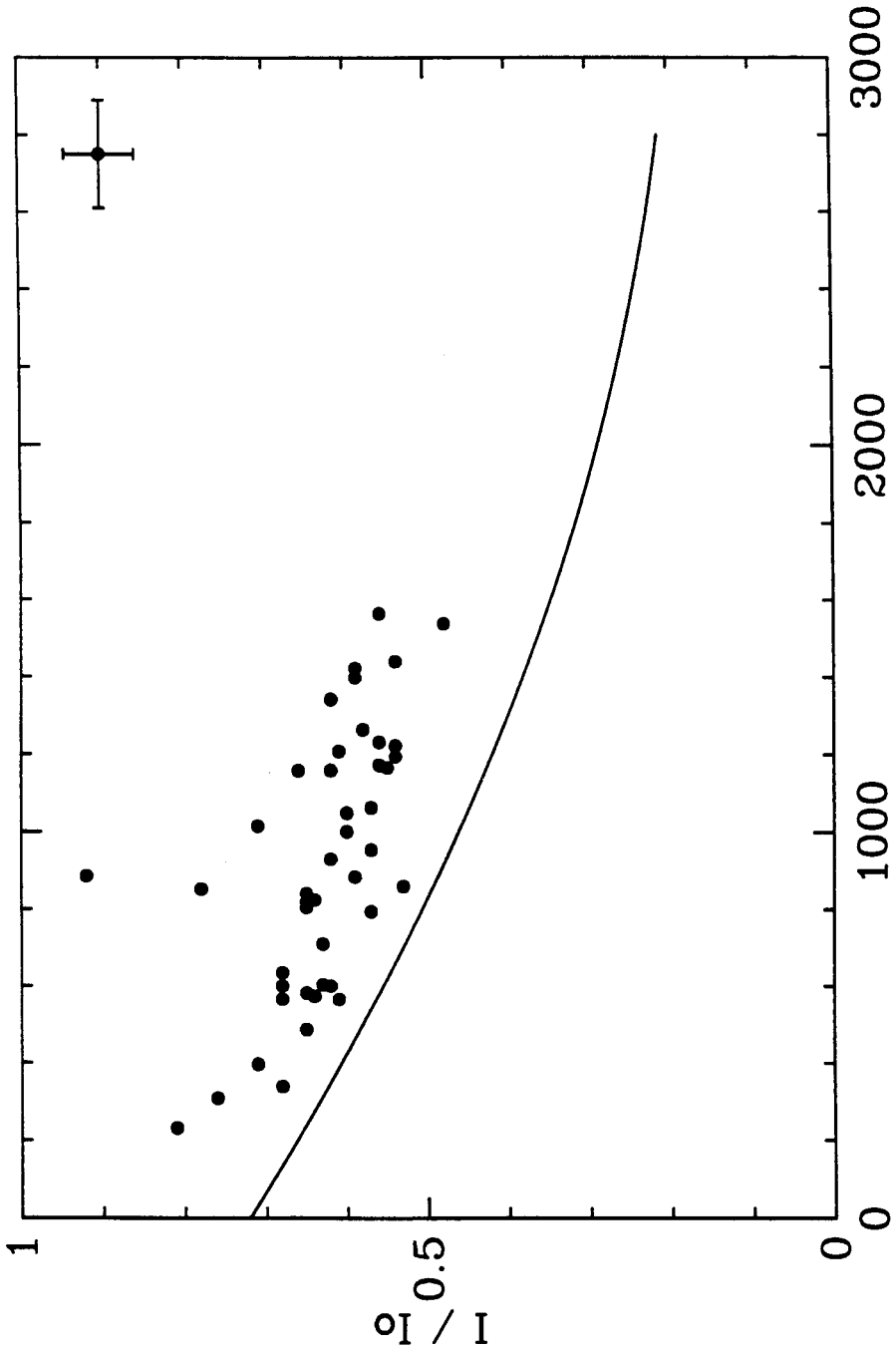

FIGURE 2

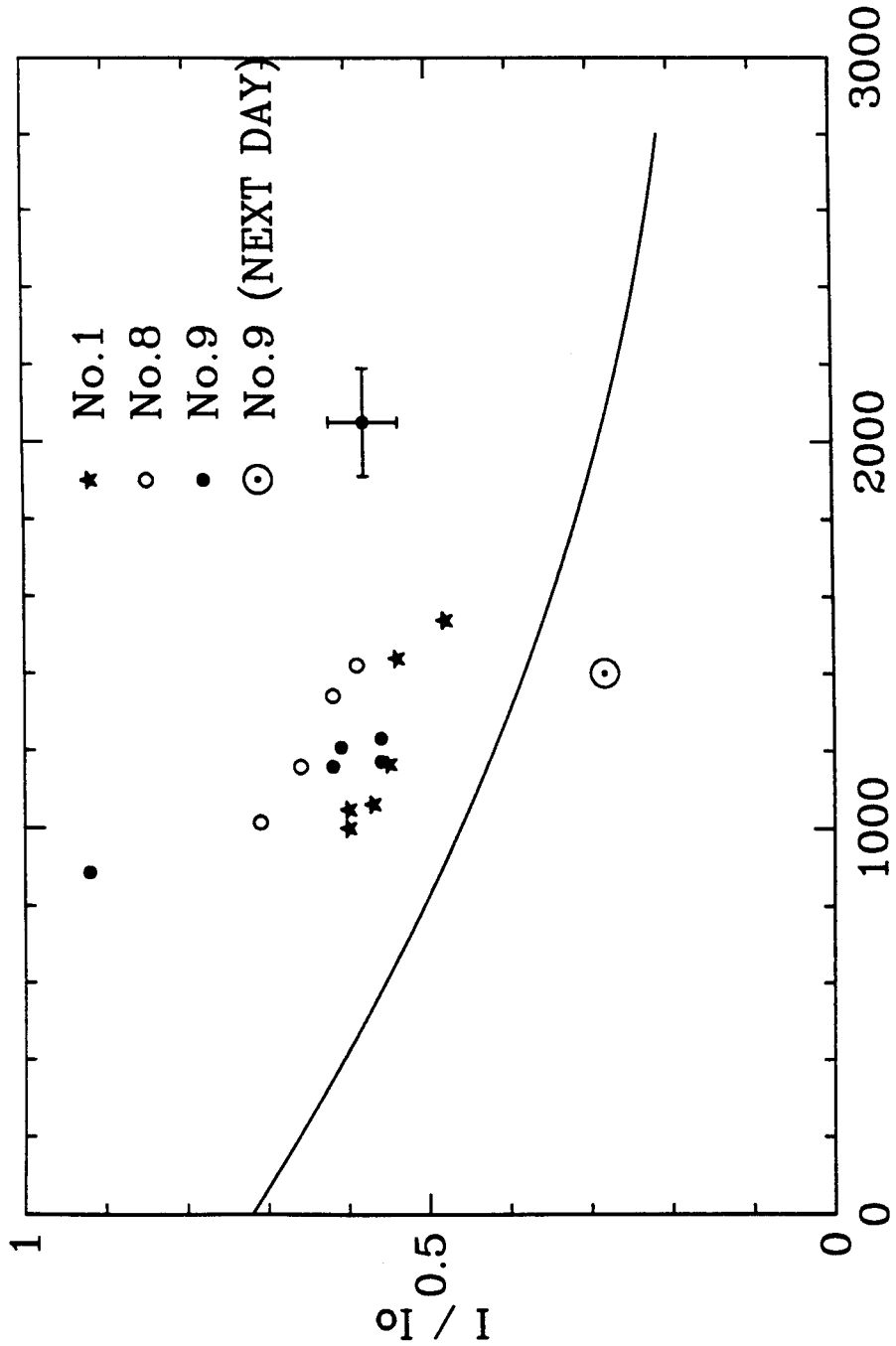

FIGURE 3

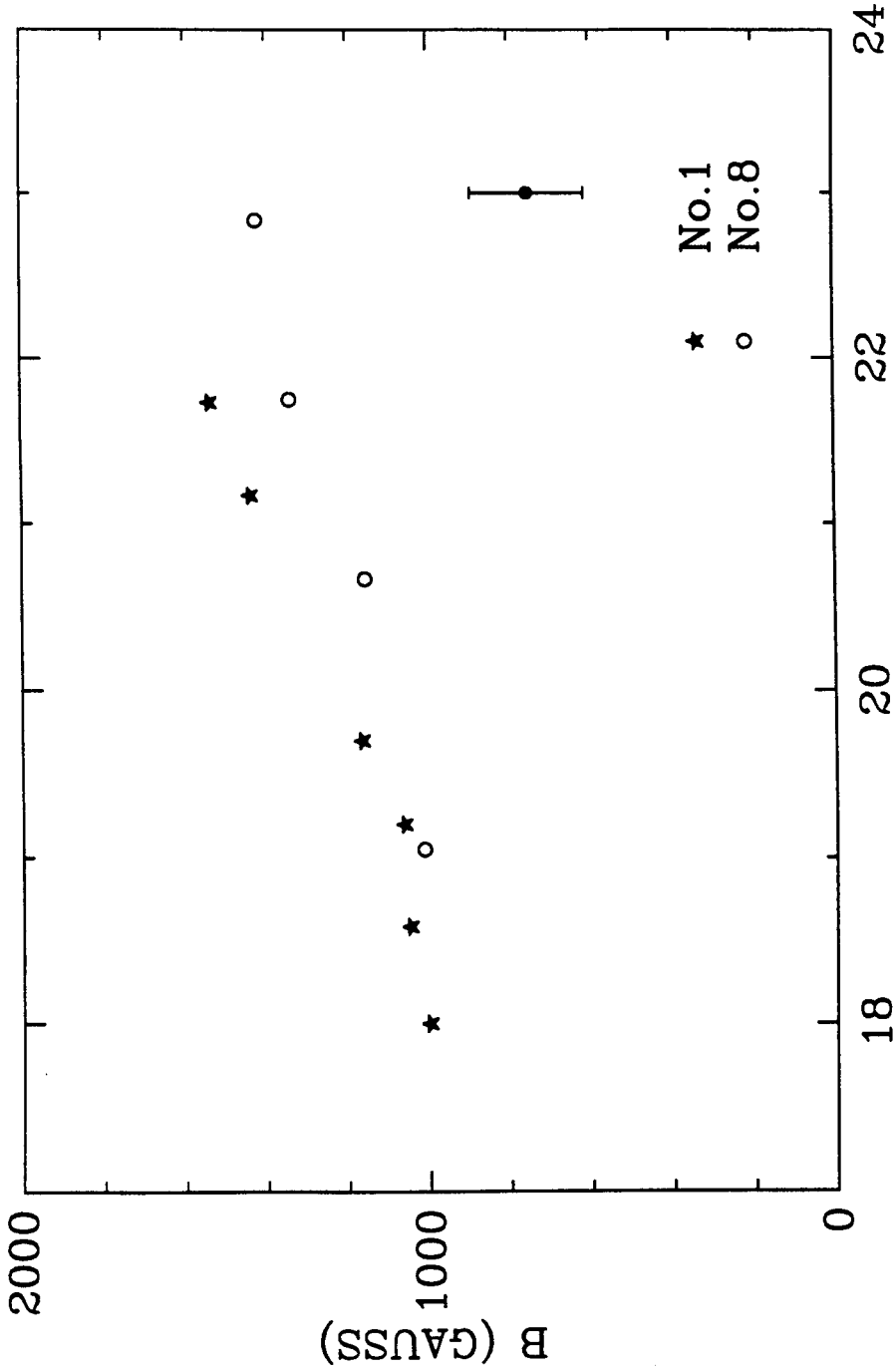

FIGURE 4

FIGURE 5

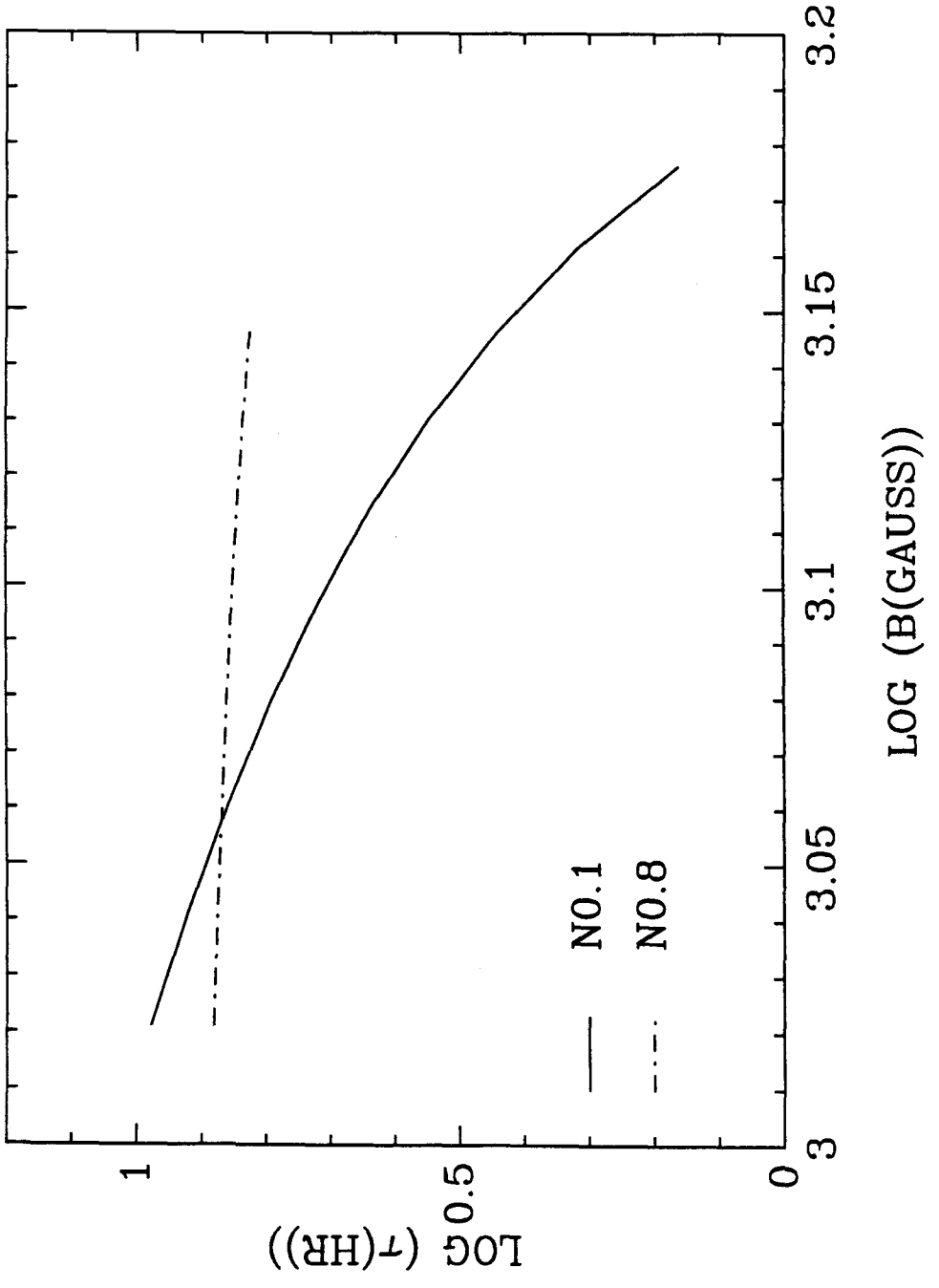

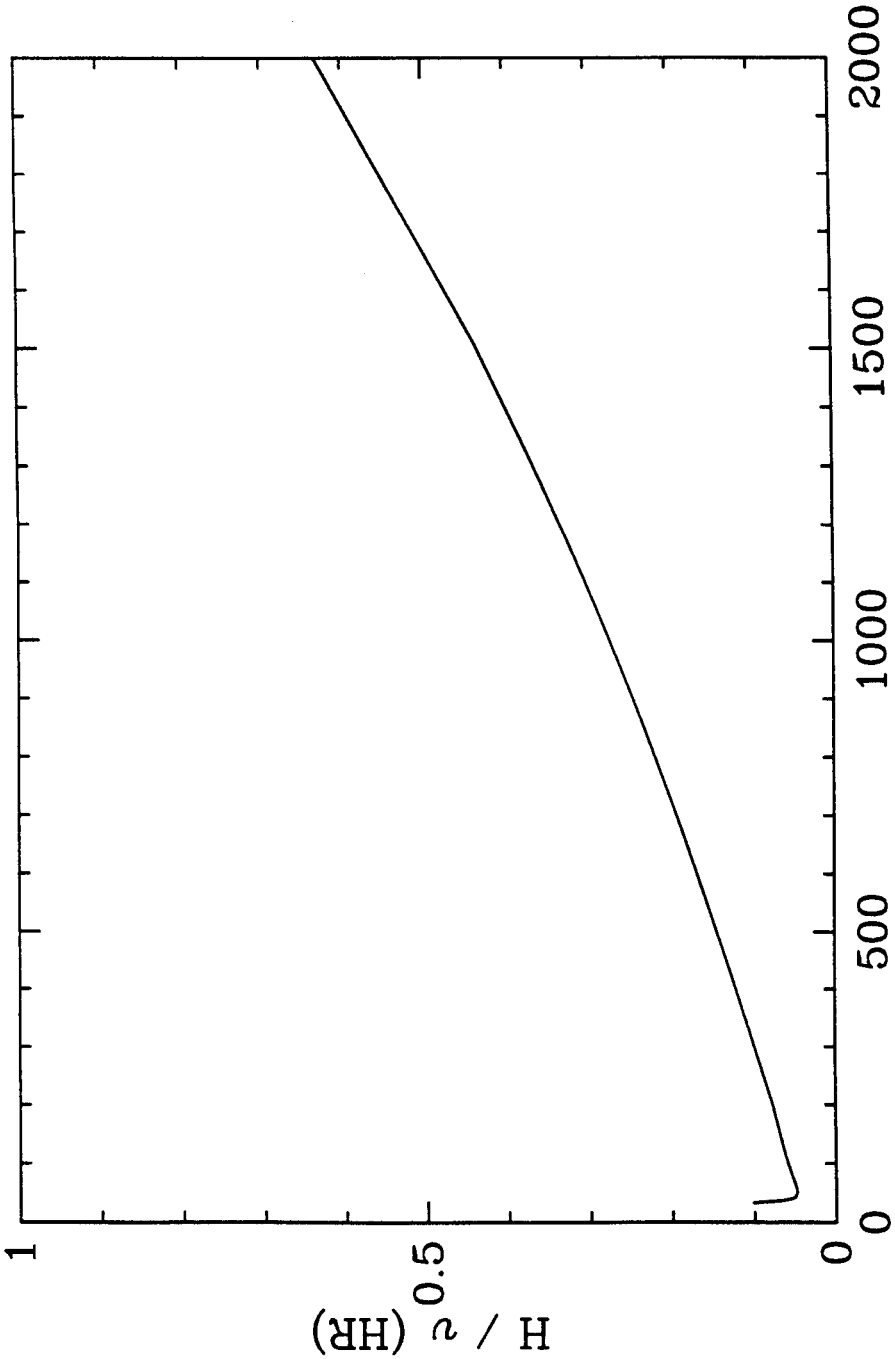

FIGURE 6

FIGURE 7

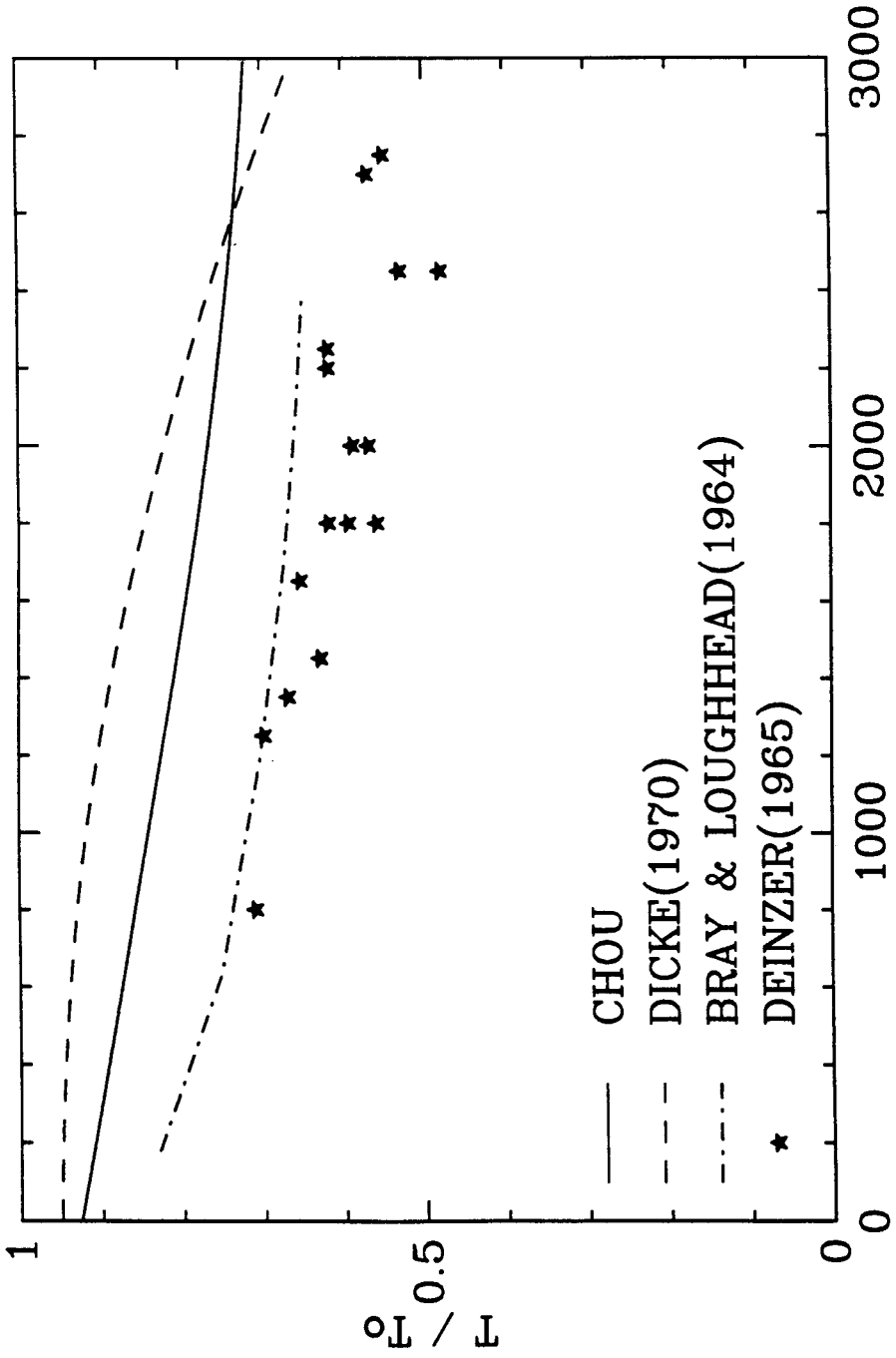
T / To
1
0.5
0
0
1000
2000
3000
B (GAUSS)
CHOU
DICKE(1970)
BRAY & LOUGHHEAD(1964)
DEINZER(1965)

CHAPTER 4

NONADIABATIC EFFECTS IN CONVECTIVE INSTABILITIES IN THIN FLUX TUBES

Submitted to Solar Physics

ABSTRACT

We study the stability of thin magnetic flux tubes in the solar convection zone. We assume that the decrease of the temperature of a thin flux tube is proportional to the increase of its field strength, based on the observational fact that sunspots with stronger magnetic field have lower effective temperature. By including this nonadiabatic effect, thin flux tubes of any field strength are stable against the convective collapse discussed by Spruit and Zweibel (1979).

I. INTRODUCTION

A stellar atmosphere is convectively unstable if the superadiabaticity, δ ($\equiv \partial \ln T/\partial \ln p - \partial \ln T/\partial \ln p|_{ad}$), is greater than zero. The magnetic field has a stabilizing effect on convection; Gough and Tayler (1966) show that in the presence of a uniform, laterally unbounded, magnetic field, a sufficient condition for stability is

$$\frac{B^2/4\pi}{B^2/4\pi + \gamma p} > \delta, \tag{1}$$

throughout the region, where B is the vertical component of magnetic field. Webb and Roberts (1978) show that this condition also holds in a slender flux tube, provided the magnetic field is constant with depth. Since the magnetic field of a thin flux tube in the solar atmosphere is not constant with depth, this condition does not determine whether a flux tube in the solar atmosphere is stable. Spruit and Zweibel (1979) show that the condition for stability of a thin flux tube in the solar atmosphere is $\beta < 1.83$ (β is the ratio of the gas pressure to the magnetic pressure), provided β is constant throughout the region, and that the perturbation is adiabatic. This implies that a flux tube with photospheric field strength less than 1083 G is hydrodynamically unstable by assuming an external pressure of $1.32 \times 10^5\, dyne/cm^2$ at the photosphere. Unno and Ando (1979) obtain a different value for the critical field strength by using different boundary conditions. Spruit (1979) shows that if the instability starts as upward motion, it behaves like normal convection in a weak dispersed field. If the instability starts as downward motion, the flux tube collapses into a new equilibrium state with stronger field strength and lower energy. This may explain the formation of small flux tubes of field strength over 1000 Gauss in the photosphere.

The above discussion is based on the assumption that the perturbation is

adiabatic. Venkatakrishnan (1985) shows that the mechanism of concentration of flux tubes by convective collapse becomes inefficient when radiative heat transport is included. In this paper, we consider a nonadiabatic effect caused by the change of the magnetic field. This is based on the observational fact that sunspots with stronger magnetic field have lower effective temperature (or less heat content). By including this nonadiabatic effect, we find that a flux tube is always stable against convective collapse.

There are two schools of thought on whether flux tubes of field strength below 1000 Gauss may exist in the photosphere. Stenflo (1973) and Harvey (1977) present evidence that all fields are stronger than 1000 Gauss. Simon and Zirker (1974), Wang et al. (1985) and Zirin (1985) present evidence for weaker fields. Our result shows that weak fields can be stable, although whether or not they actually occur is a matter to be settled by observation.

II. NONADIABATIC PROCESSES

For a thin flux tube (shown in Figure 1), whose radius is much smaller than the pressure scale height, we can ignore the transverse component of velocity and magnetic field (Roberts and Webb 1978). The equation of motion is

$$\rho \frac{dv}{dt} = -\frac{\partial p}{\partial z} - \rho g, \tag{1}$$

where v is the velocity of internal material along the flux tube. The equation of pressure balance between the inside and the outside of the flux tube is

$$p + \frac{B^2}{8\pi} = p_e, \tag{2}$$

where p_e is the external pressure. The equation for the conservation of mass and magnetic flux is

$$\frac{\partial}{\partial t}\left(\frac{\rho}{B}\right) + \frac{\partial}{\partial z}\left(v\frac{\rho}{B}\right) = 0. \tag{3}$$

The equation of state is

$$p = \frac{k\rho T}{\mu}. \tag{4}$$

Consider small perturbations from equilibrium

$$\rho = \rho_o + \rho_1,$$

$$p = p_o + p_1,$$

$$B = B_o + B_1,$$

$$v = v_o + v_1,$$

$$T = T_o + T_1,$$

where $v_0 = 0$. The schematic picture of a flux tube is shown in Figure 1. Equilibrium variables inside the tube are denoted by a subscript 0, and perturbations by a subscript 1. The linearized versions of (1) - (4) are

$$\rho_o \frac{\partial v_1}{\partial t} = -p_1' - \rho_1 g, \tag{5}$$

$$p_1 + \frac{B_o B_1}{4\pi} = 0, \tag{6}$$

$$B_o \frac{\partial \rho_1}{\partial t} - \rho_o \frac{\partial B_1}{\partial t} + (B_o \rho_o' - B_o' \rho_o) v_1 + \rho_o B_o v_1' = 0, \tag{7}$$

$$\frac{p_1}{p_o} = \frac{\rho_1}{\rho_o} + \frac{T_1}{T_o}, \tag{8}$$

where the prime denotes partial derivative with respect to the vertical coordinate z.

Observations (Deinzer 1965; Dicke 1970; Chou 1987) show that sunspots with stronger magnetic field have lower effective temperature. The mechanism to cause the low temperature is still unknown, although several possibilities, such as the Alfvén wave model, the inhibition model, and downward flow, have been proposed. Here we apply this observational fact for sunspots to thin flux tubes by assuming

that the temperature of a thin flux tube decreases if its field strength increases, even the mechanism to cause it is not clear,

$$T_1 = a \cdot B_1, \tag{9}$$

where $a = \frac{\partial T}{\partial B}$, which is assumed to be determined from the T *versus* B curve of sunspots. In the language of the Alfvén wave model, the temperature is assumed to be adjusted according to equation (9) by emitting and absorbing Alfvén waves. The increase of magnetic field could make Alfvén waves carry more energy away, and cause the temperature to decrease. Here we have assumed that the time scale to cause the temperature change by the perturbation of the field strength is much shorter than the time scale of the perturbation of the field strength. Equation (9) and the equation of state describe the local property of the perturbation. The perturbed pressure, density, and magnetic field can be related by

$$\rho_1 = -\frac{\rho_o}{B_o}\left(\frac{2}{\beta} + \frac{\partial \ln T_o}{\partial \ln B_o}\right) B_1, \tag{10}$$

$$\rho_1 = \frac{\rho_o}{p_o}\left(1 + \frac{\beta}{2} \cdot \frac{\partial \ln T_o}{\partial \ln B_o}\right) p_1, \tag{11}$$

where the value of $\frac{\partial \ln T_o}{\partial \ln B_o}$ is negative from the observations of sunspots. The sign of ρ_1 and p_1 are the same locally if $2/\beta > -\frac{\partial \ln T_o}{\partial \ln B_o}$, different if $2/\beta < -\frac{\partial \ln T_o}{\partial \ln B_o}$.

Combining equations (5), (6), (7), (8) and (9), we eliminate p_1, ρ_1, T_1, and B_1, and obtain an equation for the Fourier component v_1 of frequency ω on assuming $v_1 \propto e^{i\omega t}$. This equation is

$$v_1''(z) + A_1(z)v_1'(z) + \left\{A_2(z) + A_3(z)\omega^2\right\} v_1(z) = 0, \tag{12}$$

where

$$A_1 = -\frac{1}{\Lambda}\left(\frac{1}{\gamma} - \delta - \frac{1}{2} + \frac{\beta\epsilon}{2}\right) + \frac{2\beta'/\beta^2 - \epsilon\,(1/\gamma - \delta - 1/2)/\Lambda}{1 + 2/\beta - \epsilon},$$

$$
\begin{aligned}
A_2 &= \frac{1}{\Lambda^2}\left(\frac{1}{\gamma}-\delta-\frac{1}{2}\right)\cdot\left(\frac{1}{\gamma}-\delta-1+\frac{\beta\epsilon}{2}\right) \\
&\quad -\frac{1}{\Lambda}\left(\frac{1}{\gamma}-\delta-\frac{1}{2}\right)^2\cdot\left\{\frac{2\beta'/\beta^2-\epsilon\,(1/\gamma-\delta-1/2)/\Lambda}{1+2/\beta-\epsilon}\right\} \\
&\quad +\frac{1}{\Lambda}\left(\frac{\gamma'}{\gamma^2}+\delta'\right), \\
A_3 &= \frac{\beta}{2g\Lambda}\left(1+\frac{2}{\beta}-\epsilon\right), \\
\Lambda &= -\left(\frac{\partial \ln p_o}{\partial z}\right)^{-1}, \\
\gamma &= \frac{C_p}{C_v}, \\
\beta &= \frac{p_o}{B_o^2/8\pi}, \\
\delta &= \frac{\partial \ln T_o}{\partial \ln p_o}-\frac{\partial \ln T}{\partial \ln p}|_{ad}, \\
\epsilon &= -a\frac{B_o}{T_o} \\
&= -\frac{\partial \ln T_o}{\partial \ln B_o}.
\end{aligned}
$$

The quantity, β'/β, caused by the temperature difference between the flux tube and the exterior, can be written as (Webb and Roberts 1978)

$$\frac{\beta'}{\beta} = -\frac{\Theta}{\Lambda},$$

where

$$\Theta = \frac{\left(\frac{T_e-T}{T_e}\right)}{\left(\frac{B^2/8\pi}{pe}\right)}.$$

If the initial temperature of the flux tube is close to surrounding temperature, $\Theta \ll 1$. We will adopt this assumption in this paper.

Equation (12) can be written in the canonical form

$$\tilde{v}_1''(z) + \left(\omega^2 - \omega_o^2(z)\right) A_3(z)\,\tilde{v}_1(z) = 0, \tag{13}$$

by a transformation, $v_1 = \tilde{v}_1\, exp\{-\int(A_1/2)\,dz\}$, where

$$\omega_o^2(z) = \frac{1}{A_3(z)}\left\{\frac{1}{2}A_1'(z) + \frac{1}{4}A_1^2(z) - A_2(z)\right\}. \tag{14}$$

With the boundary conditions, $\tilde{v}_1(z_1) = \tilde{v}_1(z_2) = 0$, there exists a set of discrete solutions ω_i^2 (i = 1,2,3,...), for given values of β and ϵ. From the Sturm - Liouville theory, all of ω_i^2's are real. The flux tube is unstable for any negative ω_i^2. If all of ω_i^2's are positive, the flux tube is stable. As the first mode has the lowest frequency, ω_1^2, the stability of the flux tube is determined by the sign of ω_1^2. The flux tube is stable if ω_1^2 is positive, unstable if ω_1^2 negative.

III. NUMERICAL SOLUTIONS

To solve the eigenvalue, ω_1^2, of equation (13) numerically, we need to know the equilibrium value of Λ, γ, and δ of the flux tube. We assume that, in the equilibrium state, the quantities, Λ, γ, and δ, are the same inside and outside the flux tube at each level. We use the Harvard Smithsonian Reference Atmosphere (Gingerich et al. 1971) for $z > -33\,km$, and Spruit convective model (Spruit 1974) for $z < -33\,km$ ($z = 0$ at the photosphere and positive upward), to calculate the equilibrium value of Λ, γ, and δ for the flux tube. We also assume that, in the equilibrium state, temperature is the same inside and outside the flux tube at each level. This corresponds to β constant with depth.

The surface value of ϵ can be estimated from the curve of effective temperature *versus* magnetic field of sunspots (Deinzer 1965; Dicke 1970; Chou 1987) by assuming that the temperature in $\frac{\partial \ln T_o}{\partial \ln B_o}$ is equal to the effective temperature. It ranges about from 0 to 0.5, if $\beta > 1$. For simplicity, we assume that ϵ is constant for all z.

To get solutions appropriate to the sun, we have to choose the boundary conditions that $\tilde{v}_1(-\infty) = \tilde{v}_1(\infty) = 0$. Since superadiabaticity, which is the only factor causing convective instability, is not negligibly small only in a region of a few hundred kilometers below the photosphere, in practice, we can choose the

boundary conditions to be that $\tilde{v}_1(z_1) = \tilde{v}_1(z_2) = 0$, where z_1 and z_2 are far from the main convective region. The result would not much depend on the choice of z_1 and z_2, if they are far from the main convective region (Spruit and Zweibel 1979). Here we choose that $z_1 = 420\,km$, where $\delta < 0$, and $z_2 = -5000\,km$, where $\delta \simeq 3 \times 10^{-4}$. Both z_1 and z_2 are far from the main convective region. Different boundary conditions have been used by other authors in studying the adiabatic perturbation. Unno and Ando (1979) used the boundary condition that prescribes a relation between the velocity and its derivative at the top of the flux tube. They found that the flux tube is more unstable than one with zero velocity at the top studied by Spruit and Zweibel (1979). Venkatakrishnan (1983) also found that a flux tube with the boundary condition of nonzero velocity at the top is more unstable than one with zero velocity. Our conclusion that a flux tube is stable might change if different boundary conditions are adopted.

The eigenvalue, ω_1^2, *versus* β for various ϵ's is shown in Figure 2. The eigenvalue, ω_1^2, are positive for all β; that is, the thin flux tubes of any field strength are stable against the perturbation of motion along flux tubes.

IV. DISCUSSION

Observations show that sunspots with stronger field strength have lower temperature. Although the mechanism to cause the lower temperature is still unknown, we expect that the same mechanism also operates in thin flux tubes. In this paper, we consider a vertical thin flux tube in which the motion of the plasma is only along the flux tube; and that all internal thermodynamic variables are the same as the external ones in the equilibrium state. In the perturbed state, the decrease of the temperature of the flux tube is assumed to be proportional to the increase of its field strength. With the boundary condition that $v_1(420\,km) = v_1(-5000\,km) = 0$,

we show that the perturbation of vertical motion is stable against the convective collapse discussed by Spruit and Zweibel (1979) for any field strength. This is different from the Spruit and Zweibel result that the *adiabatic* perturbation is unstable if the field strength of the flux tube is less than a critical value, 1083 Gauss. In the adiabatic case, the plasma flowing adiabatically downward within a flux tube is cooler than its surroundings because the convective zone is superadiabatic. This temperature reduction could cause the density higher inside the flux tube, which would lead the plasma to continue to flow downward; that is, an instability would occur in the flux tube.

In the case of $\epsilon = 0$, which corresponds to the isothermal process, the temperature of the plasma flowing downward is the same as the external temperature, and the internal density is lower than the external one. Therefore, the flux tube is stable. Figure 2 also shows the expected result that the stronger the field strength is, the more stable the flux tube is (the higher the frequency is). For the case of $\epsilon \neq 0$, the process is more complicated and difficult to visualize. Since the sign of ρ_1 and B_1 are the same for $\beta > 2/\epsilon$ from equation (10), the frequency would be lower if the field strength is stronger for $\beta > 2/\epsilon$. For $\beta < 2/\epsilon$, the sign of ρ_1 and B_1 are different, and the frequency would be higher if the field strength is stronger for $\beta < 2/\epsilon$. Therefore, we expect that the lowest frequency would occur at $\beta = 2/\epsilon$. This is consistent with Figure 2, where the lowest frequency is between $\beta = 10$ and $\beta = 20$ for $\epsilon = 0.1$, and at ∞ for $\epsilon = 0$.

We have shown that flux tubes of any field strength are stable against the perturbation of motion along the flux tube, with a particular prescription that the decrease of the temperature of the flux tube is proportional to the increase of its field strength, and with the boundary condition that the perturbed velocity is zero at the both ends of the flux tube. However, if the transverse motion is taken into

account and magnetic field is not strong to inhibited the transverse motion, the flux tube might be convectively unstable. Moreover, the nonzero velocity at the top of the flux tube might allow the perturbation to grow as well.

The radius of a small flux tube is less than 300 km, which can not be resolved by present observations. The observational results indicating kilogauss rely heavily on the indirect calculation. Furthermore, it is not clear whether *all* magnetic fields at the photosphere are concentrated in small tubes of kilogauss. My result shows that, if the decrease of the temperature is proportional to the increase of the field strength, thin flux tubes of any field strength are stable against the convective collapse discussed by Spruit and Zweibel (1979), although whether or not they actually exist is a matter to be settled by observation.

REFERENCES

Chou, D. Y.: 1987, Ap. J., **312**, in press.

Deinzer, W.: 1965, *Ap. J.*, **141**, 548.

Dicke, R. H.: 1970, *Ap. J.*, **159**, 25.

Gingerich, O., Noyes, R. W., Kalkofen, W. and Cuny, Y.: 1971, *Solar Phys.*, **18**, 347.

Gough, D. O. and Tayler, R. J.: 1966, *M.N.R.A.S.*, **133**, 85.

Harvey, J. W.: 1977, *Highlight of Astronomy*, ed. E. A. Müller, **4**, Part II, p. 223.

Roberts, B. and Webb, A. R.: 1978, *Solar Phys.*, **56**, 5.

Simon, G. W. and Zirker, J. B.: 1974, *Solar Phys.*, **35**, 331.

Spruit, H. C.: 1974, *Solar Phys.*, **34**, 277.

Spruit, H. C.: 1979, *Solar Phys.*, **61**, 363.

Spruit, H. C. and Zweibel, E. G.: 1979, *Solar Phys.*, **62**, 15.

Stenflo, J. O.: 1973, *Solar Phys.*, **32**, 41.

Unno, W. and Ando, H.: 1979, *Geophys. Astrophys. Fluid Dynamics*, **12**, 107.

Venkatakrishnan, P.: 1983, *J. Astrophys. Astr.*, **4**, 135.

Venkatakrishnan, P.: 1985, *J. Astrophys. Astr.*, **6**, 21.

Wang, J., Zirin, H. and Shi, Z.: 1985, *Solar Phys.*, **98**, 241.

Webb, A. R. and Roberts, B.: 1978, *Solar Phys.*, **59**, 249.

Zirin, H.: 1985, *Aust. J. Phys.*, **38**, 961.

FIGURE CAPTIONS

FIG 1.—Schematic picture of a flux tube. Equilibrium variables inside the tube are denoted by a subscript 0, and perturbations by a subscript 1. Variables outside the tube are denoted by a subscript e. Boundary conditions are that velocity inside the tube is zero at z_1 and z_2.

FIG 2.—Square of frequency, ω^2, as a function of β for various ϵ's.

FIGURE 1

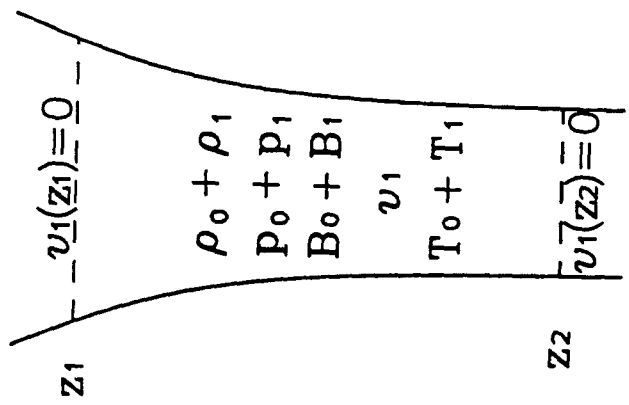
z_1
$\underline{v}_1(z_1)=\underline{0}$
$\rho_0+\rho_1$
p_0+p_1
B_0+B_1
v_1
T_0+T_1
$v_1(z_2)=0$
z_2
p_e
$B_e=0$
$v_e=0$

FIGURE 2